

# Multiple Weak Deflections and the Detection of Flattened Halos with Galaxy–Galaxy Lensing

Candace Oaxaca Wright & Tereasa G. Brainerd

*Boston University, Dept. of Astronomy, 725 Commonwealth Ave., Boston, MA 02215*

## ABSTRACT

We investigate the occurrence of multiple weak deflections in deep data sets which are used to detect galaxy–galaxy lensing. Using the galaxies in the HDF (North) for which both redshifts and rest–frame blue luminosities are known, we show that the probability for a given source galaxy to be lensed by two or more foreground galaxies exceeds 50% for source redshifts  $z_s \gtrsim 1$ , and for which the separate, individual deflections yield  $\gamma > 0.005$ . Neglecting multiple deflections when obtaining best–fitting halo parameters for the lens galaxies,  $\sigma_v^*$  and  $s^*$ , can lead to an overestimate by a factor of order 2 for the characteristic halo mass interior to a radius of  $100h^{-1}$  kpc. We also show that multiple weak deflections create systematic effects which may hinder observational efforts to use weak lensing to constrain the projected shapes of the dark matter halos of field galaxies. We model the dark matter halos of lens galaxies as truncated singular isothermal ellipsoids, and for an observational data set in which the galaxies have magnitudes in the range  $19 \lesssim I \lesssim 23$ , we find that multiple deflections result in strong correlations between the post–lensing image shapes of most foreground–background pairs of galaxies. Imposing a simple redshift cut during the analysis of the data set,  $z_d < 0.5$  and  $z_s > 0.5$ , is sufficient to reduce the correlation between the final images of lenses and sources to the point that the expected anisotropy in the weak lensing signal can be detected via a straightforward average. We conclude that previous theoretical calculations of weak lensing due to flattened dark matter halos have considerably underestimated the sizes of the observational data sets which would be required to detect this effect. In particular, for a multi–color survey in which the galaxies have apparent magnitudes of  $19 \lesssim I \lesssim 23$  and the imaging quality is modest, we find that a  $4\sigma$  detection should be obtained with a survey area of order 22 sq. deg., provided photometric redshift estimates are made for the galaxies, the typical error in  $z_{\text{phot}}$  is  $\lesssim 0.1$ , and only source galaxies with azimuthal coordinates which are within  $\pm 20^\circ$  of the lens symmetry axes are used in the data analysis.

*Subject headings:* galaxies: halos – dark matter – gravitational lensing

## 1. Introduction

The observed flatness of the rotation curves of the disks of spiral galaxies, in addition to the stellar dynamics and the hydrodynamics of hot gas in giant ellipticals, provides convincing evidence that most, if not all, large galaxies reside within massive dark matter halos (see, e.g., Fabricant & Gorenstein 1983; Stewart et al. 1984; Lauer 1985; and Fich & Tremaine 1991 and references therein). In addition, Zaritsky & White (1994) and Zaritsky et al. (1997) have used the dynamics of genuine satellites of field spirals to investigate the gravitational potentials of the halos, finding that the amount of dark matter associated with the primary galaxy is large and, specifically, they conclude that the mass contained within a radius of  $150h^{-1}$  kpc of the primary galaxy is of order  $1 - 2 \times 10^{12} h^{-1} M_{\odot}$  (here  $h$  is the present value of the Hubble parameter in units of 100 km/s/Mpc). More recently, a dynamical study of the masses of a subset of the Sloan Digital Sky Survey (SDSS) galaxies has led to similar conclusions (McKay et al. 2002). Despite the apparent ubiquity of dark halos matter around galaxies, however, the characteristic physical parameters associated with the halos, such as their shapes and physical extents, remain poorly constrained.

A number of independent investigations have, however, shown that weak, systematic gravitational lensing of background galaxies by foreground galaxies is a potentially powerful method by which the physical parameters of galaxy halos may be constrained both in the field and in rich clusters (e.g., Brainerd, Blandford & Smail 1996; Dell’Antonio & Tyson 1996; Griffiths et al. 1996; Hudson et al. 1998; Ebbels 1998; Natarajan et al. 1998, 2001; Geiger & Schneider 1999; Fischer et al. 2000; Hoekstra 2000; Jaunsen 2000; McKay et al. 2001; Smith et al. 2001; Wilson et al. 2001). This effect, known as galaxy–galaxy lensing, is too weak to be detected from the image of an individual lensed source, but since it acts coherently about the lens centers, it results in a slight preference for the images of distant source galaxies to be oriented tangentially with respect to the locations of foreground lens galaxies on the sky. Unfortunately, it is difficult to compare all of the above studies directly since the imaging quality, image deconvolution methods, and the categorization of galaxies into “lenses” and “sources” is by no means consistent amongst the investigations. The diversity of both the data and the analysis techniques notwithstanding, however, generally good agreement amongst the investigations has been found. In particular, observations of galaxy–galaxy lensing by field galaxies have yielded inferred velocity dispersions for the halos of  $L^*$  galaxies which compare well with more traditional dynamical or hydrodynamical measurements ( $\sigma_v \sim 140$  km/s to 190 km/s) and the inferred *maximum* radial extents of the

halos of  $L^*$  galaxies are very large indeed ( $\gtrsim 100h^{-1}$  kpc to  $250h^{-1}$  kpc).

With the advent of very wide-field imaging capabilities, we expect that galaxy–galaxy lensing will develop into a useful method by which fundamental questions about galaxy formation can be addressed directly. For example, Natarajan et al. (1998, 2001) and Geiger & Schneider (1999) have demonstrated that galaxy–galaxy lensing by the galaxies in rich clusters can be used to constrain the degree to which the dark matter halos of galaxies are truncated during infall. Other potential uses of galaxy–galaxy lensing include placing constraints on the evolution of the total mass–to–light ratio of galaxies (both in the field and in clusters), the morphological dependence of the halo potential (i.e., early–type versus late–type galaxies), the “bias” of light versus mass in the universe (i.e., the galaxy–mass correlation function), and even the shape of the redshift distribution of faint galaxies with redshifts in the range  $1 \lesssim z \lesssim 3$  (see, e.g., Brainerd 2002; Brainerd & Blandford 2002).

In addition to these applications, Natarajan & Refregier (2000) and Brainerd & Wright (2000) have discussed the possibility that observations of galaxy–galaxy lensing could provide direct constraints on the projected shapes of dark matter halos. Although the simple singular isothermal sphere can reproduce the flatness of the rotation curves of the disks of spiral galaxies, there are both observational and theoretical arguments in favor of halos which are flattened, rather than spherical. The observational evidence is somewhat scarce, owing to the fact that there are relatively few galaxies for which the shape of the halo potential can be probed directly via traditional methods. Nevertheless, the evidence for flattened halos is quite diverse and includes such observations as the dynamics of polar ring galaxies, the geometry of X-ray isophotes, the flaring of HI gas in spirals, the evolution of gaseous warps, and the kinematics of Population II stars in our own Galaxy. In particular, studies of disk systems which probe distances of order 15 kpc from the galactic planes suggest that the ratio of shortest to longest principle axes of the halos is  $c/a = 0.5 \pm 0.2$  (see, e.g., the comprehensive review by Sackett 1999 and references therein). Studies of a number of strong lens galaxies have also suggested that the mass distributions of the lenses are not precisely spherical. For example, Maller et al. (2000) have found that, provided the disk mass is small compared to the halo mass, the halo of the spiral galaxy which lenses the quasar B1600+434 is consistent with  $c/a = 0.53$ . In addition, the 17 strong lens systems studied by Keeton, Kochanek & Falco (1998) showed some preference for flattened mass distributions, although extremely flattened (i.e., “disky”) mass distributions were ruled out. Finally, high–resolution simulations of dissipationless cold dark matter models consistently result in markedly non–spherical galaxy halos with a mean projected ellipticity of order 0.3 (e.g., Dubinski & Carlberg 1991; Warren et al. 1992) and, therefore, from a theoretical standpoint it is not at all unreasonable to expect that the dark matter halos of galaxies should be somewhat flattened in projection.

Unlike a spherically-symmetric lens for which the gravitational lensing shear is isotropic about the lens center, the shear due to an elliptical lens is anisotropic about the lens center. Specifically, at a given angular distance,  $\theta$ , from an elliptical lens, source galaxies which are located closer to the major axis of the mass distribution of the lens will experience greater shear than sources which are located closer to the minor axis (e.g., Schneider, Ehlers & Falco 1992). Noting this well-known effect, Natarajan & Refregier (2000) and Brainerd & Wright (2000) modeled the dark matter halos of field galaxies as infinite singular isothermal ellipsoids and made rough estimates of the sizes of observational data sets which would be required to detect “anisotropic” galaxy-galaxy lensing and, hence, to constrain the net flattening of the halo population. Both studies conclude that, if the mean flattening of the halos is of order 0.3, then forthcoming wide-field surveys such as the SDSS should be able to detect this effect.

In estimating the amount of data which would be required to detect anisotropic galaxy-galaxy lensing, both Natarajan & Refregier (2000) and Brainerd & Wright (2000) made the simplifying assumption that each distant source galaxy is lensed by only one foreground galaxy. However, for a modestly deep imaging survey ( $I_{\text{lim}} \sim 23$ ), the simulations of galaxy-galaxy lensing performed by Brainerd, Blandford & Smail (1996), hereafter BBS, indicated that most of the galaxies with magnitudes in the range  $22 \lesssim I \lesssim 23$  would, in fact, have been lensed at a comparable level by two or more foreground galaxies (see, e.g., §3.5 of BBS). Therefore we expect that in a realistic data set, such “multiple deflections” may significantly affect the signal-to-noise which could be achieved when attempting to detect anisotropic galaxy-galaxy lensing.

Although BBS included a largely qualitative discussion of the importance of multiple weak deflections in deep data sets, a detailed quantitative discussion of this effect has not been published to date. Therefore, we begin this paper by demonstrating that multiple weak deflections are expected to occur with high probability within sufficiently deep data sets. For this we use the well-studied northern Hubble Deep Field, hereafter HDF-N, (Williams et al. 1996). In §2 we compute the probability distribution of weak galaxy-galaxy lensing events for the faint galaxies in the HDF-N as a function of the number of deflectors (i.e., the number of foreground lenses). In addition, we briefly investigate the effect of ignoring such multiple deflections on the values of the dark matter halo parameters that are inferred from observations of galaxy-galaxy lensing.

Having established the importance of multiple weak deflections in deep data sets, we then investigate the systematic lensing of background galaxies by foreground galaxies for a case in which the halos of the lens galaxies are modeled as truncated, singular isothermal ellipsoids. We perform Monte Carlo simulations of galaxy-galaxy lensing, including the

effects of multiple weak deflections on the final images of distant galaxies, and we compute the area of a deep ground-based imaging survey ( $I_{\text{lim}} \sim 23$ ) which would be required in order to detect anisotropic galaxy–galaxy lensing via a straightforward average of the signal. The details of the simulations, including a discussion of the lensing properties of the dark matter halos, are given in §3. The anticipated anisotropy in the galaxy–galaxy lensing signal and the results for the area of a survey which would be necessary in order to detect anisotropic galaxy–galaxy lensing in the presence of realistic observational noise are given in §4. A discussion of our results is presented in §5.

## 2. Multiple Weak Deflections in the HDF–N

The Hubble Deep Field (North) and flanking fields have been the subject of a deep redshift survey (Cohen et al. 2000) as well as an extensive multicolor photometric investigation (Hogg et al. 2000). As a result, both the redshifts,  $z$ , and the rest-frame blue luminosities,  $L_B$ , of  $\sim 600$  galaxies in this region of space are known (Cohen 2002). Therefore, it is possible to make quite a detailed theoretical prediction for the weak galaxy–galaxy lensing shear field in the region of the HDF–N and, specifically, for the probability of multiple deflections.

For simplicity, we follow the approach of BBS in their galaxy–galaxy lensing simulations and we scale the physical properties of the dark matter halos around the galaxies in the HDF–N and the flanking fields in terms of the characteristic properties associated with the halos of  $L^*$  galaxies. We let  $\sigma_v^*$  be the velocity dispersion of an  $L^*$  galaxy halo and we assume that a Tully–Fisher or Faber–Jackson type of relation will hold for each of our galaxies. We therefore have

$$\frac{\sigma_v}{\sigma_v^*} = \left( \frac{L_B}{L_B^*} \right)^{1/4}, \quad (1)$$

where  $\sigma_v$  is the velocity dispersion of a halo in which a galaxy with luminosity  $L_B$  resides.

In this section we will focus on the probability of multiple deflections and we will compute only the azimuthally-averaged galaxy–galaxy lensing shear (i.e., the mean shear within circular annuli that are centered on the lens galaxies). In this case it is sufficient to adopt a circularly-symmetric density profile for the dark matter halos and, again, we adopt the density profile used by BBS in their analysis:

$$\rho(r) = \frac{\sigma_v^2 s^s}{2\pi G r^2 (r^2 + s^2)}, \quad (2)$$

where  $G$  is Newton’s constant and  $s$  is a characteristic halo radius. (Note that since our analysis focuses solely on the weak lensing regime, it is sufficient to adopt a density profile

with a central density which is singular since the inclusion of any reasonable-sized core will not affect the weak lensing properties of the halos at all.) As in BBS we assume that the total mass-to-light ratio of a galaxy is constant independent of its luminosity and, therefore, the radii of the halos of galaxies with  $L_B \neq L_B^*$  scale with the radii of the halos of  $L_B^*$  galaxies according to:

$$\frac{s}{s^*} = \left( \frac{L_B}{L_B^*} \right)^{1/2}. \quad (3)$$

Throughout we adopt fiducial values of  $\sigma_v^* = 156$  km/s and  $s^* = 100h^{-1}$  kpc for the halos of  $L_B^*$  galaxies (i.e., comparable to the characteristic parameters which have been inferred from previous studies of galaxy-galaxy lensing).

Having made these assumptions, we can make predictions for the galaxy-galaxy lensing shear field within the region of the HDF-N that would be generated by the  $\sim 600$  galaxies in Cohen (2002). These objects include not only galaxies in the HDF-N, but also galaxies in the flanking fields and, due to the substantial masses of some of the galaxies in the flanking fields, their weak lensing effects may influence the shear field inside the much smaller region of the HDF-N itself. We therefore include the flanking field galaxies in all of our calculations for the weak shear field inside the HDF-N.

Here our goal is to quantify the probability that a given faint galaxy will be weakly-lensed by one or more foreground galaxies. This probability will, of course, be a strong function of the actual value of the shear,  $\gamma$ , due to a given weak lensing deflection. That is, it is much more likely for a distant galaxy to be lensed by a foreground galaxy which produces a shear of  $\gamma \sim 0.001$  than, say, a shear of  $\gamma \sim 0.01$ . Therefore, in order to discuss the number of weak deflections that a given source galaxy is likely to encounter, we must first decide what minimum value of  $\gamma$  qualifies as a “significant” deflection.

A typical value for the net shear due to galaxy-galaxy lensing is  $\gamma \sim 0.005$  (see, e.g., the observational papers cited in the Introduction) and we use this value of  $\gamma$  as a baseline for computing the number of weak lensing deflections that source galaxies undergo. Specifically, we compute  $P(N_D)$ , the probability that a given galaxy is lensed by  $N_D$  foreground galaxies (i.e., “deflectors”) where each *individual deflection* gives rise to a shear of  $\gamma \geq 0.005$ . That is,  $P(N_D = 2)$  is the probability that a given galaxy has been lensed by two individual foreground galaxies, each of which lensed the distant galaxy at a level which is comparable to or greater than the expected net shear due to galaxy-galaxy lensing.

Shown in Fig. 1 is the theoretical probability distribution function,  $P(N_D)$ , for source galaxies in the HDF-N with redshifts of  $z_s$ . In order to produce this result, source galaxies were placed at random locations within the HDF-N and were assigned specific redshifts,  $z_s$ . Note that since the angular clustering of cosmologically-distant galaxies is observed to be

quite weak (e.g., Infante & Pritchett 1995; Villumsen, Freudling & da Costa 1997; Brainerd & Smail 1998) and since BBS found that the inclusion of the intrinsic clustering of the faint galaxies in their sample made no measurable difference to the predicted galaxy–galaxy lensing signal, the use of random location for our source galaxies is reasonably well–justified.

Using the scaling relations above, the individual values of  $\gamma$  due to each one of the galaxies in Cohen (2002) is computed for the source galaxies and a probability distribution for individual deflections with  $\gamma > 0.005$  is assembled. Results are shown in Fig. 1 for three different cosmologies: open ( $\Omega_0 = 0.3$ ,  $\Lambda_0 = 0$ ,  $H_0 = 60$  km/s/Mpc), flat Lambda-dominated ( $\Omega_0 = 0.3$ ,  $\Lambda_0 = 0.7$ ,  $H_0 = 60$  km/s/Mpc), and Einstein–de Sitter ( $\Omega_0 = 1.0$ ,  $\Lambda_0 = 0$ ,  $H_0 = 60$  km/s/Mpc). The probability distributions are nearly independent of the cosmology, which is unsurprising since the galaxy–galaxy lensing shear has only a weak cosmology dependence (see, e.g., BBS §3.6).

For a source galaxy in the HDF–N which is located at a redshift of  $z_s = 0.5$ , the probability of being lensed by even one foreground galaxy is quite small. This is due to the fact that the median redshift of the galaxies in Cohen (2002) is of order 0.6 and, hence, many of the “lens” galaxies are actually more distant than the “source” galaxies. At a redshift of  $z_s = 1$ , however, the probability that a source galaxy has been lensed at a significant level by *two or more* foreground galaxies is of order 50%. At source redshifts of  $z_s = 1.25$ , 1.5, and 1.75, the probability of a source galaxy encountering multiple deflections of  $\gamma > 0.005$  increases to of order 70%, 85%, and 90%, respectively. Therefore, we expect that in a deep data set for which the median redshift is  $\gtrsim 1$ , multiple weak deflections of a substantial magnitude are very likely to have occurred. Of course, in the case of individual deflections for which  $\gamma < 0.005$ , the probability of comparable multiple deflections occurring at any given source redshift will be greater than the results shown in Fig. 1.

A major goal of studies of galaxy–galaxy lensing is to constrain the nature of the dark matter halos of the lens galaxies. That is, one wishes to use observations of the galaxy–galaxy lensing shear to measure the values of the parameters  $\sigma_v^*$  and  $s^*$  above. However, it is clear from Fig. 1 that multiple deflections will likely occur in deep data sets and, therefore, they should be included in calculations which attempt to infer  $\sigma_v^*$  and  $s^*$  from a detection of galaxy–galaxy lensing. To assess the degree of error in  $\sigma_v^*$  and  $s^*$  which would be caused by not including multiple deflections, we compute  $\gamma(\theta)$ , the theoretical mean shear as a function of lens–source separation in the HDF–N, for two distinct cases: (i) all of the weak deflections are included in the determination of the net shear experienced by each source galaxy, and (ii) only the deflection due to the closest lens (in projection on the sky) is used to determine the shear. That is, in case (ii) we ignore all of the multiple deflections and we assume that the nearest neighbor lens galaxy is the only lens. This is motivated by the fact

that for a singular isothermal potential the shear decreases as  $\gamma(\theta) \propto \theta^{-1}$  and, therefore, in the simplistic case of lenses being confined to a single plane in redshift space and sources being confined to another plane in redshift space, the nearest neighbor lens is likely to be the only “important” lens.

The magnitude of the mean shear due to galaxy–galaxy lensing is, of course, strongly–dependent upon the depth of the source sample and here we restrict our analysis to source galaxies with  $I < 23$  (corresponding to a median redshift of order 0.85). Although the completeness limit of the HDF–N extends far below this magnitude,  $I_{\text{lim}} \sim 23$  is comparable to the limiting magnitude of most of the deeper data sets which have so far been used to study galaxy–galaxy lensing. Unfortunately, due to the small area of the field there are relatively few galaxies in the HDF–N data which satisfy our limiting magnitude requirements (only of order 30 galaxies with known redshifts). Therefore, an accurate prediction of the effects of multiple deflections on the galaxy–galaxy lensing shear cannot be obtained simply by using the observed HDF–N galaxies. Instead, we must generate Monte Carlo source galaxy catalogs which reproduce the observed faint galaxy number counts and for which we adopt a parameterized redshift distribution. As in BBS, we use a redshift distribution of the form

$$P(z|I) = \frac{\beta z^2 \exp[-(z/z_0)^\beta]}{\Gamma(3/\beta)z_0^3} \quad (4)$$

(e.g., Baugh & Efstathiou 1993), which is in good agreement with both the no–evolution model and with the observed redshift distribution of galaxies with  $19 \leq I \leq 22$  obtained from the Canada France Redshift Survey (e.g., LeFèvre et al. 1996). Here

$$z_0 = k_z[z_m + z'_m(I - I_m)], \quad (5)$$

where  $z_m$  is the median redshift,  $I_m$  is the median  $I$ -band magnitude, and  $z'_m$  is the derivative of the median redshift with respect to  $I$ . Extrapolating the results of the CFRS to a sample of galaxies with  $19 \leq I \leq 25$  we have that  $z_m = 0.86$ ,  $z'_m = 0.15$ ,  $k_z = 0.8$ , and  $\beta = 1.5$ . A total of 6250 Monte Carlo realizations of the source galaxy distribution were generated, and the shear experienced by each of the sources was computed.

Since galaxy–galaxy lensing occurs in the weak regime (i.e.,  $|\vec{\gamma}| \ll 1$ ), the net shear experienced by any source galaxy which has been weakly–lensed by more than one foreground galaxy can be computed simply as the (complex) vector sum of the shears induced by each of the individual lenses (e.g., Schneider, Ehlers & Falco 1992). Therefore, the net shear experienced by a given source galaxy after having been lensed by  $M$  weak lenses is given by:

$$\vec{\gamma} \equiv \gamma_1 + i\gamma_2 = \sum_{j=1}^M \gamma_{1,j} + i \sum_{j=1}^M \gamma_{2,j}, \quad (6)$$



where  $\gamma_{1,j}$  is the real component of the shear due to lens  $j$  and  $\gamma_{2,j}$  is the imaginary component. For our calculations of the net shear due to multiple weak deflections, we include all deflections,  $j$ , encountered by each source galaxy (i.e., not just those deflections for which  $\gamma_j > 0.005$ ).

Shown in Fig. 2 is the variation of the mean shear with lens–source separation, both with and without the inclusion of multiple deflections. As before, we take  $\sigma_v^* = 156$  km/s and  $s^* = 100h^{-1}$  kpc and, for simplicity, we have only considered the case of an open universe. (Since the galaxy–galaxy lensing signal is so weakly–dependent upon the cosmology, there is no significant loss of generality from this choice.) On scales  $> 1''$ , Fig. 2 shows that there is a substantial systematic error (of order 50%) in the mean shear when multiple deflections are ignored in the calculation. As a result, if one were to model the true shear field with a theoretical shear field that did not include multiple deflections, substantial systematic errors in the best–fitting values of  $\sigma_v^*$  and  $s^*$  would result. We demonstrate this in Fig. 3, where we compare the actual shear produced by the HDF–N galaxies (i.e., the solid squares in Fig. 2) to the shear that one obtains for single–deflection calculations which use various values of  $\sigma_v^*$  and  $s^*$ . Formally, the best–fitting values from the single–deflection calculations are  $\sigma_v^* = 198$  km/s and  $s^* = 435h^{-1}$  kpc, which are very much larger than the input values of 156 km/s and  $100h^{-1}$  kpc. (Note, however, that the galaxy–galaxy lensing shear is relatively insensitive to the radii of the halos and, so, for a given value of  $s^*$ ,  $\chi^2$  is nearly identical for all values of  $s^*$  which exceed  $100h^{-1}$  kpc. See also §3.6 of BBS.) Neglecting multiple deflections in the process of constraining  $\sigma_v^*$  and  $s^*$  leads, therefore, to a formal estimate of the mass of the halo of an  $L^*$  galaxy which is a factor of  $\sim 2$  too large within a radius of  $100h^{-1}$  kpc (e.g., BBS equation 3.4).

We therefore conclude that the effects of multiple weak deflections can be quite important in the accurate prediction of theoretical galaxy–galaxy lensing shear fields, and in the determination of the characteristic parameters which are associated with the halos of the lens galaxies. We now turn to theoretical calculations of shear fields caused by flattened dark matter halos, and for which we have explicitly included all of the multiple deflections.

### 3. Galaxy–Galaxy Lensing with Flattened Halos

While the HDF–N is a useful field for demonstrating the likelihood and effects of multiple weak deflections, it is nevertheless an extremely small field and one for which the effects of halo flattening will not be convincingly detected in the galaxy–galaxy lensing signal. We, therefore, have constructed large Monte Carlo galaxy catalogs in order to investigate weak lensing by non–spherical galaxy halos. In the following subsections we outline the details of

the galaxy catalogs and their weak lensing properties.

### 3.1. Luminous Properties of the Galaxies

The Monte Carlo galaxy catalogs are designed to reproduce a number of observational constraints on the faint galaxy population:

- the number counts of faint galaxies,  $\frac{d \log N}{dm}$ , to a limiting magnitude of  $I_{\text{lim}} = 25$
- the shape of the redshift distribution of faint galaxies,  $N(z)$ , extrapolated to  $I_{\text{lim}} = 25$
- the distribution of intrinsic shapes (i.e., the unlensed equivalent image ellipses of the light distribution of the sources), as obtained from deep imaging with HST

Each galaxy catalog is generated within a  $40' \times 40'$  region of sky and for simplicity we adopt an open cosmology with  $H_0 = 60$  km/s/Mpc,  $\Omega_0 = 0.3$ ,  $\Lambda_0 = 0$ . A total of 500 independent catalogs were generated and were then used to compute the mean galaxy–galaxy lensing signal which would occur if the dark matter halos of the galaxies were substantially flattened.

As in §2, all galaxies in our catalogs are assigned random locations on the frame. Each galaxy is also assigned an apparent magnitude,  $19 < I < 25$ , which is drawn from the deep  $I$ -band number counts obtained by Smail et al. (1995). This results in a number density of 60 galaxies per square arcminute in the simulations. In addition, each galaxy is assigned an intrinsic (i.e., unlensed) position angle which is drawn at random from  $-\frac{\pi}{2} \leq \phi \leq \frac{\pi}{2}$ . That is, we assume that in the absence of gravitational lensing, the orientations of the major axes of the images of the distant galaxies are randomly distributed. The galaxies are also assigned intrinsic shapes,  $\tau \equiv (a^2 - b^2)/(2ab)$ , drawn from the probability distribution

$$P(\tau) = A\tau \exp[-(\tau/0.036)^{0.54}] \quad (7)$$

which was obtained by Ebbels (1998) using 94 deep archival HST images of blank fields. Here  $a$  is the major axis of the (unlensed) equivalent image ellipse of a galaxy and  $b$  is the minor axis.

Each galaxy is assigned a redshift based upon its apparent magnitude, drawn from equation (4) in §2, and each galaxy is also assigned an intrinsic luminosity,  $L$ , according to:

$$\frac{L}{L^*} = \left( \frac{H_0 D_d}{c} \right) (1+z)^{3+\alpha} 10^{0.4(22.9-I)}, \quad (8)$$

(see, e.g., BBS). Here  $D_d$  is the angular diameter distance to the galaxy,  $z$  is its redshift,  $I$  is its apparent magnitude, and the parameter  $\alpha$  is the slope of the spectral energy distribution:

$$\alpha = -\frac{d \log_{10} L_\nu}{d\nu}. \quad (9)$$

For simplicity we adopt the mean slope,  $\alpha = 0.42$ , between the  $R$  and  $B$  bands which was found in the Caltech Faint Galaxy Redshift Survey (Cohen et al. 1999ab).

### 3.2. Gravitational Properties of the Galaxies

Having assigned all of the intrinsic properties of the galaxies which are associated with the light distribution, we then assign the intrinsic properties which are associated with the distribution of the mass. Each galaxy is assumed to reside within a dark matter halo which can be fairly represented as a truncated singular isothermal ellipsoid. Following Kormann et al. (1994), the surface mass densities of the dark matter halos are given by

$$\Sigma(\rho) = \frac{\sigma_v^2 \sqrt{f}}{2G} \left( \frac{1}{\rho} - \frac{1}{\sqrt{\rho^2 + x_t^2}} \right), \quad (10)$$

where  $\sigma_v$  is the line of sight velocity dispersion,  $f$  is the axis ratio of the mass distribution as projected on the sky ( $0 < f \leq 1$ ),  $x_t$  is a truncation radius,  $G$  is Newton’s constant, and  $\rho$  is a generalized elliptical radius defined such that  $\rho^2 = x_1^2 + f^2 x_2^2$ . Here  $x_1$  and  $x_2$  are Cartesian coordinates measured, respectively, along the minor and major axes of the projected mass distribution of the halo. In the limiting case of a round lens (i.e.,  $f \rightarrow 1$ ), the total mass of the halo becomes

$$M_{\text{tot}} = \frac{\pi \sigma_v^2 x_t}{G}, \quad (11)$$

which is identical to the halo mass model adopted by BBS.

Provided a galaxy is in a state of dynamical equilibrium (i.e., it has not undergone a recent collision or merger), it is reasonable to expect that, in projection on the sky, the position angle of major axis of the mass distribution will be aligned well with the (unlensed) major axis of the light distribution. In addition, work by Keeton, Kochanek & Falco (1998) and Kochanek (2001) has shown that the mass and light in strong lens galaxies is aligned quite well. Therefore, we assign a position angle to each halo (as projected on the sky) which is identical to the intrinsic position angle that was assigned to its light distribution in §3.1. However, we do not assign identical intrinsic ellipticities to both the mass and light distributions. Instead, the ellipticity of each galaxy’s halo is drawn from a probability distribution which is constructed from current observational constraints on the shapes of

galaxy halos. Specifically, from principle moment analyses in which, by definition,  $a > b > c$ , the distribution of halo shapes seems to favor  $c/a = 0.5 \pm 0.2$  and  $b/a \gtrsim 0.8$  (see, e.g., Sackett 1999). To generate the distribution of projected ellipticities of the halos, then, we construct ten million ellipsoids in which the values of  $b/a$  are drawn from a uniform distribution  $0.8 \leq b/a \leq 1.0$  and the values of  $c/a$  are drawn from a Gaussian distribution with a mean of 0.5 and a standard deviation of 0.2. Each ellipsoid is then projected onto a plane which is oriented perpendicularly to a randomly-chosen line of sight and the distribution of the projected axis ratios of the ellipsoids is computed. The result is shown in Fig. 4, where the mean and median ellipticities of the distribution are both of order 0.3 and we use the convention that  $\epsilon \equiv 1 - b/a = 1 - f$ .

As in §2, we scale the physical properties of the galaxy halos in terms of the characteristic properties associated with the halos of  $L^*$  galaxies:  $\frac{\sigma_v}{\sigma_v^*} = \left(\frac{L}{L^*}\right)^{1/4}$  and  $\frac{x_t}{x_t^*} = \left(\frac{L}{L^*}\right)^{1/2}$ . Again, we adopt a fiducial value of  $\sigma_v^* = 156$  km/s for the velocity dispersion of the halo of an  $L^*$  galaxy and a corresponding truncation radius of  $x_t^* = 100h^{-1}$  kpc.

### 3.3. Lensing Properties of the Halos

The convergence of the lenses is given by

$$\kappa(\rho) = \frac{\sigma_v^2 \sqrt{f}}{2G\Sigma_c} \left( \frac{1}{\rho} - \frac{1}{\sqrt{\rho^2 + x_t^2}} \right), \quad (12)$$

where  $\Sigma_c \equiv \left(\frac{4\pi G}{c^2} \frac{D_d D_{ds}}{D_s}\right)^{-1}$  is the “critical surface mass density”,  $D_d$  is the angular diameter distance of the lens,  $D_s$  is the angular diameter distance of the source and  $D_{ds}$  is the angular diameter distance between the lens and the source. The real and imaginary components of the shear due to a lens with a projected axis ratio of  $f$  can be derived straightforwardly by using equations (63abc) of Kormann et al. (1994):

$$\gamma_1 = \frac{\sigma_v^2 \sqrt{f}}{2G\Sigma_c} \left[ -\frac{\cos(2\varphi)}{\rho} - \{f^2(x_1^2 - x_2^2) - (1 - f^2)x_t^2\} \mathcal{P} \right] \quad (13)$$

$$\gamma_2 = \frac{\sigma_v^2 \sqrt{f}}{2G\Sigma_c} \left[ -\frac{\sin(2\varphi)}{\rho} - 2f^2 x_1 x_2 \mathcal{P} \right] \quad (14)$$

where

$$\mathcal{P} \equiv \frac{x_1^2 + f^4 x_2^2 - (1 + f^2)(\rho^2 + x_t^2) + 2f x_t \sqrt{\rho^2 + x_t^2}}{\sqrt{\rho^2 + x_t^2} [f^4 r^4 - 2f^2(1 - f^2)x_t^2(x_1^2 - x_2^2) + (1 - f^2)^2 x_t^4]}. \quad (15)$$

Recall from eqn. (10) above that  $x_1$  and  $x_2$  are Cartesian coordinates measured along the minor and major axes of the lens, respectively. In order to maintain consistency with the

notation of Kormann et al. (1994), here we have also introduced a polar coordinate system, centered on the lens, with radial coordinate  $r \equiv \sqrt{x_1^2 + x_2^2}$  and polar angle,  $\varphi$ , defined such that  $x_1 = r \cos \varphi$  and  $x_2 = r \sin \varphi$ .

It is clear from equations (12) through (15) that, unlike a circularly symmetric lens for which the magnitude of the shear depends only upon the angular distance from the lens center, the shear due to an elliptical lens is a function of both the angular distance from the lens center *and* the azimuthal coordinate of the source as measured with respect to the symmetry axes of the lens. At a given angular distance,  $\theta$ , from the lens center, the magnitude of the shear is greatest for sources located nearest to the major axis of the lens and least for sources located nearest to the minor axis of the lens. Hence, in a given radial annulus which is centered on the lens, the mean shear experienced by sources whose azimuthal coordinate,  $\varphi$ , places them within  $\pm N^\circ$  of the major axis of the lens will be greater than that for sources whose azimuthal coordinate,  $\varphi$ , places them within  $\pm N^\circ$  of the minor axis. As a shorthand notation, we refer to the magnitude of the mean shear experienced by sources whose azimuthal coordinates place them within  $\pm N^\circ$  of the minor axis of the lens as  $\langle \gamma^- \rangle$ . Similarly, we refer to the magnitude of the mean shear experienced by sources whose azimuthal coordinates place them within  $\pm N^\circ$  of the major axis of the lens as  $\langle \gamma^+ \rangle$ . For clarity, we illustrate our use of this notation in Fig. 5.

For each galaxy in our simulations we define an “intrinsic” shape parameter,  $\vec{\gamma}_i$ , which describes the image of the galaxy prior to being lensed:

$$\vec{\gamma}_i \equiv \frac{a - b}{a + b} e^{2i\phi}, \quad (16)$$

where  $a$  and  $b$  are the intrinsic major and minor axes of the light distribution and  $\phi$  is its intrinsic position angle. Since we are again dealing only with the weak lensing regime, the final shape of a galaxy,  $\vec{\gamma}_f$ , after having been lensed by  $M$  foreground galaxies is given by:

$$\vec{\gamma}_f = \vec{\gamma}_i + \sum_{j=1}^M \vec{\gamma}_j, \quad (17)$$

where  $\vec{\gamma}_j$  is the weak shear due to lens  $j$ .

For each galaxy,  $i$ , which has a redshift of  $z_i$ , all other galaxies,  $j$ , with redshifts  $z_j < z_i$  can formally be considered to be lenses of galaxy  $i$ . However, since the galaxy–galaxy lensing signal drops off steeply with projected lens–source separation on the sky (i.e.,  $|\vec{\gamma}(\theta)| \propto \theta^{-1}$  on scales,  $\theta$ , which are less than or of order the angle subtended by the lens, and  $|\vec{\gamma}(\theta)|$  falls off even more steeply on scales larger than that subtended by the lens), we do not actually compute the weak shear due to all of the foreground galaxies,  $j$ , which are within the full

$40' \times 40'$  region of the simulation. Instead, to reduce the run time of the simulations, we simply compute the net shear on each (source) galaxy  $i$  due to all (lens) galaxies  $j$  which are located within  $150''$  of galaxy  $i$ . Increasing the maximum lens–source separation to  $300''$  has a negligible effect ( $< 0.01|\vec{\gamma}_f|$ ) on the net shear computed for each of the source galaxies.

#### 4. Results

Using the final image shapes of the galaxies,  $\vec{\gamma}_f$ , we compute the angular dependence of the mean value of the shear experienced by sources located closest to the minor axes of lens galaxies,  $\langle \gamma^- \rangle$ , as well as the mean value of the shear experienced by sources located closest to the major axes of lens galaxies,  $\langle \gamma^+ \rangle$  (e.g., Fig. 5). Clearly, in the case of isolated lenses for which the position angle of the *mass* distribution of the lens (i.e., the position angle of the halo as projected on the sky) is known precisely, we expect  $\langle \gamma^- \rangle < \langle \gamma^+ \rangle$  on all angular scales,  $\theta$ , which are less than or of order the angular scale subtended by the halos. Of course, on angular scales which are substantially larger than that subtended by the halos, the ratio  $\langle \gamma^- \rangle / \langle \gamma^+ \rangle$  will approach unity since, for all intents and purposes, the truncated elliptical lens begins to act similarly to a point mass lens.

Here we restrict our analysis to galaxies for which  $19 < I < 23$ , since a limiting magnitude of order  $I = 23$  can be achieved in a reasonable amount of observing time with large ground–based telescopes, and because this limiting magnitude is comparable to the deeper data sets which have been used to detect galaxy–galaxy lensing. We do, however, include the effects of systematic lensing due to galaxies with  $23 \leq I \leq 25$  on the images of galaxies with  $I < 23$  since the redshifts of some galaxies with  $I \geq 23$  will, in fact, be smaller than the redshifts of some galaxies with  $I < 23$  (e.g., equation (4) above). In addition, because of the finite area of the fields (1600 square arcminutes each), we restrict our computation of  $\langle \gamma^- \rangle$  and  $\langle \gamma^+ \rangle$  to only those galaxies which are located within the central  $30' \times 30'$  region of each simulation. This is done in order to avoid errors in the calculation of the mean shear which would occur simply due to boundary effects caused by the fact that source galaxies located close to the edges of the simulations will not have been lensed by objects which would, in a larger simulation, exist just outside our  $40' \times 40'$  frame.

In all cases below, we compute the mean shear only on scales greater than  $\theta = 5''$ . This is identical to the inner radius imposed by BBS in their analysis and it insures that in a realistic data set the “source” galaxies in the analysis will be located more than 7 scale lengths from the “lens” galaxies (see, e.g., BBS). This, in turn, insures that systematic errors due to overlapping isophotes of lens and source galaxies should not occur in a realistic observational data set.

#### 4.1. No Observational Noise

We first compute the angular dependence of  $\langle\gamma^-\rangle$  and  $\langle\gamma^+\rangle$  in the limit of truly “ideal” data. That is, from the simulations we have precise knowledge of the orientation of the major axes of all of the halos, the redshifts of the galaxies, and the final shape parameters,  $\vec{\gamma}_f$ , of the images of the galaxies after they have been lensed by all foreground galaxies. The only source of “noise” in the data, therefore, is simply that due to the intrinsic ellipticity distribution of the galaxy shapes.

For all foreground galaxies,  $j$ , located at an angular distance  $\theta$  from all background galaxies,  $i$  (i.e.,  $z_j < z_i$ ), we compute the net tangential shear of the background galaxies using the individual values of  $\vec{\gamma}_f$  which were obtained in the simulations. For all background galaxies located within  $\pm N^\circ$  of the symmetry axes of the halos, then, we compute the angular dependence of  $\langle\gamma^-\rangle$ ,  $\langle\gamma^+\rangle$ , and the ratio  $\langle\gamma^-\rangle / \langle\gamma^+\rangle$  as a function of differential lens–source separation on the sky. The results are shown in Fig. 6, where the left panels show results for  $N = 45^\circ$ , and the right panels show results for  $N = 20^\circ$ .

As expected, the variation of  $\langle\gamma^-\rangle$  and  $\langle\gamma^+\rangle$  with differential lens–source separation is well-fitted by a broken power law. That is, on scales,  $\theta$ , which are less than or of order the angle subtended by the lenses, the mean shear should decrease roughly as  $\theta^{-1}$  since we have adopted an isothermal density profile. On scales larger than the truncation radius, a steepening in the variation of the mean shear with angular separation ought to occur and this, indeed, is the case. The changes in slope which are shown in the top panels of Fig. 6 occur at  $\theta \simeq 33''$  which, unsurprisingly, corresponds to the mean projected value of the truncation radii of the halos,  $\langle x_t \rangle \simeq 33''$ . For sources located within  $\pm 45^\circ$  of the symmetry axes of lenses, the change in slope is of order  $-0.5$  (i.e., steeper than the slope for an isothermal lens, but not quite as steep as that for a point mass lens). Again as expected, the variation of the ratio  $\langle\gamma^-\rangle / \langle\gamma^+\rangle$  as a function of differential lens–source separation is less than unity on small angular scales and approaches unity on scales considerably larger than the mean projected value of the halo truncation radii.

For the purposes of planning possible future observational investigations, we are interested in estimating the size of a deep imaging survey which would be required to detect the effects of flattened halos on the galaxy–galaxy lensing signal. To do this we define an “anisotropy parameter”,

$$\mathcal{A} \equiv 1 - \frac{\langle\gamma^-\rangle}{\langle\gamma^+\rangle}, \quad (18)$$

and, again for the case of truly ideal data, we compute the signal–to–noise in a measurement of  $\mathcal{A}$  as a function of the area of the survey. Shown in Fig. 7 are the results for lens–source separations of  $5'' \leq \theta \leq \theta_{\text{out}}$ , where  $\theta_{\text{out}} = 35'', 75'',$  and  $135''$  for the cases of  $N = 45^\circ$

(left panels) and  $N = 20^\circ$  (right panels). For the case of  $N = 20^\circ$ , the values of the anisotropy parameter are  $\mathcal{A} = 0.24, 0.20, 0.18$  for  $\theta_{\text{out}} = 35'', 75'', 135''$  and a  $4\sigma$  detection of  $\mathcal{A}$  should be obtained with surveys of area 3.5, 5.0, and 9.0 square degrees, respectively. For the case of  $N = 45^\circ$ , the values of the anisotropy parameter are  $\mathcal{A} = 0.15, 0.13, 0.11$  for  $\theta_{\text{out}} = 35'', 75'', 135''$  and a  $4\sigma$  detection of  $\mathcal{A}$  should be obtained with surveys of area 5.0, 7.0, and 14.5 square degrees, respectively.

## 4.2. Lensing–Induced Image Correlations

In the above subsection, we computed  $\langle\gamma^-\rangle$  and  $\langle\gamma^+\rangle$  relative to the actual symmetry axes of the halos of the lens galaxies themselves. That is,  $N$  was specifically measured relative to the major and minor axes of the *halos* as seen in projection. Of course, in a real data set one must measure  $N$  relative to the major and minor axes of the *light* distribution of the lens galaxies and, to some extent, the position angle of a lens galaxy’s equivalent image ellipse will differ from its intrinsic position angle due to the fact that lens galaxies with redshifts  $z_i$  will have been weakly–lensed by foreground galaxies with redshifts  $z_j < z_i$ . For a typical galaxy in our simulation, the misalignment between the intrinsic position angle of the galaxy and its final post–lensing position angle is of order  $5^\circ$  or less. This, clearly, is a source of intrinsic noise in the determination of  $N$  which one might think would be very small indeed (particularly for values of  $N \gg 5^\circ$ ). However, as we show below, this slight deflection of the position angles of the lens galaxies away from their intrinsic position angles (i.e., those which were aligned with the halo major axes *a priori*) induces a substantial systematic error in the values of  $\langle\gamma^-\rangle$  and  $\langle\gamma^+\rangle$  when these quantities are computed relative to the post–lensing position angles of the images of the lens galaxies.

Shown in Fig. 8 is the angular dependence of  $\langle\gamma^-\rangle$ ,  $\langle\gamma^+\rangle$ , and  $\langle\gamma^-\rangle / \langle\gamma^+\rangle$  for  $N = 45^\circ$  (left panels) and  $N = 20^\circ$  (right panels), where  $N$  has been measured relative to the final, observed position angles of the lens galaxies. That is, the sole difference between Fig. 8 and Fig. 6 is that here  $N$  is measured relative to the final, post-lensing position angles of the images of the lens galaxies, whereas previously we measured  $N$  relative to the intrinsic position angles of the lenses. In Fig. 8 we see quite a striking trend: on scales larger than about  $10''$  the values of  $\langle\gamma^-\rangle$  actually exceed those of  $\langle\gamma^+\rangle$  and, hence, the ratio  $\langle\gamma^-\rangle / \langle\gamma^+\rangle$  is greater than unity.

In the limit of single deflections for each source galaxy, and for the case of isolated lens galaxies which are not themselves lensed by any foreground object, we always expect  $\langle\gamma^-\rangle / \langle\gamma^+\rangle$  to be less than unity on small scales. However, due to the fact that our galaxies are broadly distributed in redshift and we have taken full account of all weak lensing events



for all of the galaxies, we clearly do not have this idealized limiting case. Rather, consider the case of 3 galaxies with redshifts  $z_1 < z_2 < z_3$ . If the galaxy at  $z_3$  is weakly-lensed by both of the galaxies at  $z_2$  and  $z_1$ , and the galaxy at  $z_2$  is also weakly-lensed by the galaxy at  $z_1$ , then correlated alignments of the post-lensing images of the galaxies at  $z_2$  and  $z_3$  will occur. This, in turn, will cause  $\langle \gamma^- \rangle / \langle \gamma^+ \rangle$  as measured relative to the final image of the lens at  $z_2$  to be greater than unity (effectively by decreasing the net ellipticity of sources at  $z_3$  which are closest to the projected major axis of the halo of the lens at  $z_2$  and, simultaneously, increasing the net ellipticity of sources at  $z_3$  which are closest to the minor axis of the halo).

We quantify this effect in our simulations using a correlation function of the image shapes,

$$C_{\gamma\gamma}(\theta) \equiv \langle \vec{\gamma}_1 \cdot \vec{\gamma}_2^* \rangle \quad (19)$$

where the mean value is computed for all foreground-background pairs of galaxies separated by angles  $\theta \pm \delta\theta/2$  on the sky (see, e.g., Blandford et al. 1991). Here  $\vec{\gamma}_1$  is the image shape of a galaxy with redshift  $z_1$  and  $\vec{\gamma}_2^*$  is the complex conjugate of the image shape of a galaxy with redshift  $z_2 > z_1$  (see, e.g., equations 16 and 17 above). This function measures the degree to which the images of galaxy 1 and galaxy 2 are aligned with one another and in the limit of no systematic alignments between images 1 and 2,  $C_{\gamma\gamma}(\theta)$  is identically zero on all scales.

Shown in the top panel of Fig. 9 is the function  $C_{\gamma\gamma}(\theta)$ , computed using the intrinsic shape parameters,  $\vec{\gamma}_i$ , of all galaxies with magnitudes in the range  $19 < I < 23$ . As expected,  $C_{\gamma\gamma}(\theta)$  is consistent with zero on all scales since all galaxies are assigned intrinsic shape parameters which are drawn at random at the start of each simulation. Shown in the middle panel of Fig. 9 is  $C_{\gamma\gamma}(\theta)$  computed using the final shape parameters for all galaxies with  $19 < I < 23$  (i.e., the objects which we have used to measure  $\langle \gamma^- \rangle$  and  $\langle \gamma^+ \rangle$  in Figs. 6 and 8). Here there is clearly a net correlation of foreground-background image shapes on scales  $\theta \lesssim 60''$  and a slight anti-correlation on larger scales. It is this small-scale correlation of the final image shapes between foreground and background galaxies which is responsible for the ratio  $\langle \gamma^- \rangle / \langle \gamma^+ \rangle$  being greater than unity in Fig. 8. That is, the effect of multiple weak lensing events on *pairs* of lenses and sources is to cause a slight tendency for the images of lenses and sources to be preferentially aligned with each other on angular scales  $\lesssim 60''$  in our simulations.

This effect will, of course, be strongest for foreground-background pairs in which the redshifts of the foreground and background objects are fairly similar (i.e., each of the two objects is likely to be multiply-lensed by an identical number of foreground objects). Therefore, it should be possible to reduce the effect of correlated lens-source shape parameters by restricting our analysis to lens redshifts,  $z_d$ , which are relatively smaller than the source

redshifts,  $z_s$ . We find that this does, indeed, occur when we restrict our analysis to the following cases: (i)  $z_d < 0.1$ ,  $z_s > 0.1$ ; (ii)  $z_d < 0.2$ ,  $z_s > 0.2$ ; (iii)  $z_d < 0.5$ ,  $z_s > 0.5$ . Redshift cuts using  $z_d < 0.1$  and  $z_d < 0.2$  result in values of  $\langle \gamma^- \rangle / \langle \gamma^+ \rangle$  which are less than unity, but which require excessively wide fields in order to detect our anisotropy parameter,  $\mathcal{A}$ , at a significant level. A redshift cut at  $z_d < 0.5$ , however, largely eliminates any correlation between the values of  $\vec{\gamma}_f$  for all foreground–background pairs of galaxies (see the bottom panel of Fig. 9) and still allows a significant detection of  $\mathcal{A}$  with only moderate–sized data sets.

### 4.3. Effects of Observational Noise

In the above sections we have demonstrated that in the limit of imaging data which contains no observational noise whatsoever, it is possible in principle to detect the effects of flattened halos on the galaxy–galaxy lensing signal. That is, the only noise for which we have accounted so far is the “intrinsic” noise associated with the fact that the galaxy images have a broad distribution of intrinsic ellipticities and that multiple weak lensing events can cause the images of foreground–background pairs of galaxies to be preferentially aligned with one another.

Here we include the effects of realistic observational noise in our analysis in order to determine whether or not a detection of galaxy–galaxy lensing by flattened halos would be feasible with ground–based imaging data of modest quality. It is unlikely that spectroscopic redshifts would be available for all of the galaxies in an observational data set which has a depth comparable to our simulations; however, photometric redshifts could certainly be obtained in a multi–color data set and these could be used for the purposes of lens–source separation. Photometric redshifts are, of course, not exact and this will introduce some level of noise into the analysis. In addition, seeing, sky noise, and pixellation effects introduce noise into the observed, final image shapes (i.e., the observed values of  $\vec{\gamma}_f$ ) and they, therefore, degrade the galaxy–galaxy lensing signal itself.

We model the effects of noise which would be introduced by the use of photometric redshifts (as opposed to spectroscopic redshifts) by adding an error term to each galaxy’s actual redshift:

$$z_{\text{obs}} = z_{\text{in}} + \delta z, \tag{20}$$

where  $z_{\text{in}}$  is the intrinsic redshift assigned to the galaxy at the start of the simulation and  $\delta z$  is an error term drawn from a Gaussian distribution with zero mean and a standard deviation of 0.1. This is in reasonable agreement with the accuracy of photometric redshifts found by Hogg et al. (1998) who conducted a blind test of the predictions of several photometric

redshift algorithms against the actual spectroscopic redshifts of galaxies in the HDF–N and found that for 68% of the galaxies the error in the photometric redshift was  $\lesssim 0.1$ .

We model the effects of noise introduced in the imaging process by adding appropriate errors to the final, observed position angles of the galaxies. This is identical to the approach followed by BBS in their simulations of galaxy–galaxy lensing and is motivated to a large extent by simplicity. That is, although there will certainly be a finite error associated with the measurement of the ellipticity of a galaxy’s image, we choose to incorporate all of the observational error in a measurement of  $\vec{\gamma}_f$  into an error in the final, observed position angle since it is largely the degree of tangential alignment of the source galaxies relative to the lens galaxies which gives rise to the significance of a detection of galaxy–galaxy lensing.

The magnitudes of the galaxies used by BBS in their observational investigation of galaxy–galaxy lensing,  $20 \leq r \leq 24$ , were very similar to those adopted for our simulations and we use the results of matched galaxy catalogs from substacks of the BBS data set to assign errors in the position angles of the galaxies in our simulations. From substacks of the data, BBS noted that the typical error in the position angle of a faint galaxy is dependent upon not only the magnitude of the galaxy but also its ellipticity, with the error being most significant for the roundest galaxies (see, e.g., Table 2 of BBS). We extend the original analysis of BBS to galaxies which are brighter than those which are tabulated in their paper and in Table 1 we show the typical errors in the position angles of galaxies with  $19 < I < 23$  as a function of both  $I$ –magnitude and ellipticity,  $\epsilon$ . We also note that the median seeing in the BBS data was  $0.9''$  FWHM and no attempt was made by BBS to deconvolve the images, so the data should be fairly representative of the imaging quality which could be achieved under modest observing conditions.

For each galaxy in the simulation, then, we assign an error to the final, observed (i.e., post–lensing) position angle based upon the galaxy’s apparent magnitude and its ellipticity after having been lensed by all foreground objects. The error is assigned from a Gaussian distribution with zero mean and the appropriate standard deviation from Table 1. Thus, we now have a set of objects with redshifts ( $z_{\text{obs}}$ ) and final shape parameters ( $\vec{\gamma}_f^{\text{obs}}$ ) which have been “corrupted” by the inclusion of moderate errors.

Using these corrupted redshifts and final shape parameters, then, we re–compute the signal–to–noise which can be achieved in a measurement of our anisotropy parameter,  $\mathcal{A}$ , as a function of the area of the survey. Again, to reduce the effects of correlated shape parameters of foreground and background galaxies, we use only lens galaxies with  $z_d^{\text{obs}} < 0.5$  and source galaxies with  $z_s^{\text{obs}} > 0.5$  in the analysis. The results are shown in Fig. 10 where, as in Fig. 7, the left panel corresponds to the case in which  $N = 45^\circ$  and the right panel corresponds to the case in which  $N = 20^\circ$ . Not unexpectedly, we find that for a given survey area the

signal-to-noise in a measurement of  $\mathcal{A}$  decreases significantly when moderate amounts of observational noise are included in the calculation. Nevertheless, when the signal is averaged over relatively small angular scales,  $5'' \leq \theta \leq 35''$ , a  $4\sigma$  detection of  $\mathcal{A}$  can be achieved with a data set of order 22 square degrees in the case of  $N = 20^\circ$  and with a data set of order 32 square degrees in the case of  $N = 45^\circ$ .

#### 4.4. Weighted Means

In the previous sections we have used only simple, unweighted means in our calculations of  $\langle\gamma^-\rangle$  and  $\langle\gamma^+\rangle$ . However, as our two illustrative cases of  $N = 20^\circ$  and  $N = 45^\circ$  demonstrate, the “signal” (i.e., the level of anisotropy) is greatest for sources located closest to the symmetry axes of lenses and will, of course, be nearly identical for all sources which have azimuthal coordinates,  $\varphi$ , which are close to  $45^\circ$ . In principle, therefore, one should consider computing  $\langle\gamma^-\rangle$  and  $\langle\gamma^+\rangle$  using all sources within  $N = 45^\circ$  via a weighted mean which would weight sources with  $N \ll 45^\circ$  strongly, while largely discarding sources with  $N \simeq 45^\circ$  from the calculation.

In this section we compute  $\langle\gamma^-\rangle$  and  $\langle\gamma^+\rangle$  using simple weighted means where the weight applied to the image of galaxy  $i$  is of the form:

$$w_i = N^{-1/n}, \tag{21}$$

where  $n = 2, 3, 4, \dots, 9$ . For brevity, we show only results for the case of the noisy data used in §4.3 (i.e., noise added to both the image shapes and the redshifts), and a fiducial analysis annulus of  $5'' \leq \theta \leq 35''$ . Results for signal-to-noise as a function of survey area as obtained from the weighted means are shown in Fig. 11, where they are directly compared to the results of the previous unweighted means (i.e., Fig. 10).

From Fig. 11, it is clear that when all sources within  $N = 45^\circ$  of the lens symmetry axes are used, this weighting scheme yields an improvement in the S/N over the unweighted mean for the case of  $n > 4$ . However, increasing  $n$  beyond a value of 4 does not increase the S/N substantially for a given survey area and, in fact, the simple unweighted mean which uses all sources within  $N = 20^\circ$  of the lens symmetry axes yields the largest signal to noise values.

## 5. Discussion

We have used the well-studied HDF–N to show that the probability of multiple weak deflections due to galaxy–galaxy lensing is significant in a deep data set ( $I_{\text{lim}} \sim 23$ ). Using a fiducial model in which the halos of  $L^*$  galaxies have characteristic velocity dispersions of 156 km/s and outer radii of  $100h^{-1}$  kpc, we have shown that neglecting multiple weak deflections when predicting the galaxy–galaxy lensing shear field results in a substantial underestimate of the mean shear on scales  $> 1''$ . This, in turn, leads to an overestimate of the mass of the halo of an  $L^*$  galaxy by a factor of order 2 interior to a radius of  $100h^{-1}$  kpc.

We have also used Monte Carlo simulations of galaxy–galaxy lensing by flattened dark matter halos to compute the signal–to–noise which might be achieved for a measurement of  $\mathcal{A} \equiv 1 - \langle \gamma^- \rangle / \langle \gamma^+ \rangle$ . For modest degree of observational noise (including errors in photometric redshifts and in the determination of the final image shapes) in a data set for which the galaxy magnitudes are in the range  $19 < I < 23$ , we find that a simple unweighted mean in the computations of  $\langle \gamma^- \rangle$  and  $\langle \gamma^+ \rangle$  should yield a significant detection of the weak lensing signal due to flattened halos provided the data set is sufficiently wide. Multiple weak deflections (i.e., weak lensing of background lens–source pairs by foreground galaxies) do, however, tend to cause alignments between the final images of lenses and sources, which complicates the detection of the expected anisotropy in the galaxy–galaxy lensing signal. A simple redshift cut of  $z_d < 0.5$ ,  $z_s > 0.5$  is sufficient to break this correlation, however. Imposing such a redshift cut, and restricting our unweighted mean to sources within  $N = 20^\circ$  of the lens symmetry axes, we find that a  $4\sigma$  detection of the anisotropy parameter can be obtained with a data set of order 22 square degrees. If all sources within  $N = 45^\circ$  of the lens symmetry axes are used, the required survey area increases to of order 32 square degrees for a  $4\sigma$  detection.

Two previous investigations, Natarajan & Refregier (2000) and Brainerd & Wright (2000), have also made predictions for the sizes of data sets which would be necessary in order to detect the anisotropic signature of systematic weak lensing by flattened dark matter halos. Neither of these investigations included the effects of multiple weak deflections on the lensing signal and both considered only the very simple case in which all galaxy halos are modeled as infinite singular isothermal ellipsoids with identical projected ellipticities,  $\epsilon$ .

Brainerd & Wright (2000) used the observed signal–to–noise in the galaxy–galaxy lensing signal obtained by BBS to estimate the size of a data set with imaging characteristics similar to the BBS data which would be required in order to detect galaxy–galaxy lensing by flattened halos. They computed the anisotropy parameter,  $\mathcal{A}$ , for the case of  $N = 45^\circ$  and used unweighted means in the computations of  $\langle \gamma^- \rangle$  and  $\langle \gamma^+ \rangle$ . For halo mass ellipticities of  $\epsilon = 0.3$ , and using all sources within  $N = 45^\circ$  of the lens symmetry axes, Brainerd & Wright

(2000) concluded that a mere 1.25 square degrees of imaging data similar to that of BBS would be sufficient to yield a  $4\sigma$  detection of weak lensing by flattened halos when averaged over lens–source separations of  $5'' \leq \theta \leq 35''$ . This estimate is, however, a factor of order 25 too small compared to the results of the simulations discussed here (i.e., left panel of Fig. 10).

Natarajan & Refregier (2000) used a complimentary approach to predict that, in the absence of observational noise, the signal–to–noise which could be achieved in a measurement of:

$$\epsilon_\kappa = \frac{a^2 - b^2}{a^2 + b^2} \quad (22)$$

is given by:

$$\left(\frac{S}{N}\right)_{\epsilon_\kappa} \simeq 4.6 \left(\frac{\epsilon_\kappa}{0.3}\right) \left(\frac{\alpha}{0.5''}\right) \left(\frac{n_b}{1.5 \text{ arcmin}^{-2}}\right)^{1/2} \left(\frac{n_f}{0.035 \text{ arcmin}^{-2}}\right)^{1/2} \left(\frac{0.3}{\sigma_\epsilon}\right) \left(\frac{A}{1000 \text{ deg}^2}\right)^{1/2} \quad (23)$$

where  $\alpha$  is the Einstein radius,  $n_b$  is the number of background galaxies,  $n_f$  is the number of foreground galaxies,  $\sigma_\epsilon^2$  is the variance in the intrinsic ellipticity distribution of galaxies ( $\sim 0.3^2$ ), and  $A$  is the area of the survey. For a data set similar to that of BBS (i.e., similar to the type of data set investigated in this paper and in Brainerd & Wright 2000), we have that  $\alpha \sim 0.17''$ ,  $n_b = 7 \text{ arcmin}^{-2}$ , and  $n_f = 6 \text{ arcmin}^{-2}$  (see, e.g., BBS). Adopting these values of  $\alpha$ ,  $n_b$ , and  $n_f$  as being representative, then, equation (23) predicts that for a value of  $b/a = 0.7$  (i.e.,  $\epsilon = 0.3$  in our notation and  $\epsilon_\kappa = 0.34$  in the notation of Natarajan and Refregier), a  $4\sigma$  detection of weak lensing by flattened halos should be detectable in a survey with an area of order 6 square degrees. Again, compared with the predictions of our simulations, this is a considerable underestimate of the size of the data set which would be needed in order to detect the anisotropic lensing signal at a significant level.

The primary motivation for studies of galaxy–galaxy lensing has, of course, been its promise to place strong statistical constraints on the physical parameters of the halos of galaxies. This motivation is well–justified because of the fact that weak lensing provides a probe of the gravitational potentials of the halos of the lens galaxies up to very large physical radii (on the order of  $100h^{-1}$  kpc or so), where dynamical and hydrodynamical tracers of the potential are very unlikely to be found for the vast majority of the galaxies in the universe. To date, the published studies of galaxy–galaxy lensing by field galaxies have attempted to constrain the depths of the potential wells of the halos of the lens galaxies and their typical outer scale radii, but they are only just beginning to address the shapes of the halos. In a very preliminary, but nevertheless tantalizing, study, Hoekstra, Yee & Gladders (2002) have used a maximum likelihood technique to constrain the shapes of the halos of early–type galaxies in the Red–Sequence Cluster Survey and they find that they can rule out spherical

halos at the 99% confidence level. Although not yet a definitive result, this is certainly encouraging for future studies which aim to constrain halo shapes via weak lensing.

Here we have explored galaxy–galaxy lensing by field galaxies with flattened halos and we have concluded that the resulting weak lensing signal should be detectable in deep, wide, multi-color data sets with modest imaging quality. That is, provided the halos have a median ellipticity of order 0.3, we find that an anisotropy in the weak lensing signal (i.e.,  $\langle\gamma^-\rangle$  vs.  $\langle\gamma^+\rangle$ ) is detectable via an appropriate strategy in the data analysis. However, in closing we caution that this is not identical to a direct measurement of the mean flattening of the halo population; it is, rather, an indicator that the halos are not spherically–symmetric on average. If all galaxy halos were infinite singular isothermal ellipsoids with identical ellipticities in projection on the sky, and all galaxy images were weakly–lensed by one and only one foreground galaxy, then it would be very straightforward to turn a single measurement of  $\langle\gamma^-\rangle / \langle\gamma^+\rangle$ , or equivalently  $\mathcal{A}$ , into a direct measurement of  $\epsilon$  (see, e.g., Brainerd 2002 and Brainerd & Wright 2000). It is, of course, not realistic to suppose that all halos have identical ellipticities in projection and this, combined with the need to remove lensing–induced correlations between the final shapes of lenses and sources will certainly necessitate the use of detailed Monte Carlo simulations to translate any future measurements of anisotropies in the galaxy–galaxy lensing signal into constraints on the mean flattening of the halos of field galaxies.

### Acknowledgments

Support under NSF contracts AST-9616968 (TGB and COW), AST-0098572 (TGB), an NSF Graduate Minority Fellowship (COW), and a generous allocation of resources at Boston University’s Scientific Computing and Visualization Center are gratefully acknowledged.

## REFERENCES

- Baugh, C. M. & Efstathiou, G. 1993, MNRAS, 265, 145
- Blandford, R. D., Saust, A.-B., Brainerd, T. G., & Villumsen, J. V. 1991, MNRAS, 251, 600
- Brainerd, T. G. 2002, in “New Cosmological Data and the Values of the Fundamental Parameters”, proceedings of IAU Symposium 201, eds. A. Lasenby & A. Wilkinson, in press
- Brainerd, T.G., Blandford, R.D., & Smail, I. 1996, ApJ, 466, 623 (BBS)
- Brainerd, T. G. & Blandford, R. D. 2002, in “Dark Matter and Gravitational Lensing”, eds. F. Courbin & D. Minniti, Springer-Verlag, in press
- Brainerd, T. G. & Smail, I. 1998, ApJ, 494, L137
- Brainerd, T.G., & Wright, C.O. 2000, astro-ph/0006281
- Cohen, J. 2002, ApJ, 567, 672
- Cohen, J., Hogg, D. W., Blandford, R., Cowie, L. L., Hu, E., Songaila, A., Shopbell, P., & Richberg, K. 2000, ApJ, 538, 29
- Cohen, J., Blandford, R., Hogg, D.W., Pahre, M.A., & Shopbell, P.L. 1999a ApJ, 512, 30
- Cohen, J., Hogg, D.W., Pahre, M.A., Blandford, R., Shopbell, P.L., & Richberg, K. 1999b ApJS, 120, 171
- Dell’Antonio, I.P. & Tyson, J.A. 1996, ApJ, 473, L17
- Dubinski, J. & Carlberg, R. 1991, ApJ, 378, 496
- Ebbels, T. 1998, PhD Thesis, University of Cambridge
- Fabricant, D. & Gorenstein, P. 1983, ApJ, 267, 535
- Fich, M. & Tremaine, S. 1991, ARA&A, 29, 409
- Fischer, P., McKay, T.A., Sheldon, E., Connolly, A., Stebbins, A., Frieman, J.A., Jain, B., Joffe, M., Johnston, D., Bernstein, G., Annis, J., Bahcall, N.A., Brinkmann, J., Carr, M.A., Csabai, I., Gunn, J.E., Hennessy, G.S., Hindsley, R.B., Hull, C., Ivezić, Z., Knapp, G. R., Limmongkol, S., Lupton, R.H., Munn, J.A., Nash, T., Newberg, H.J., Owen, R., Pier, J.R., Rockosi, C.M., Schneider, D.P., Smith, J.A., Stoughton, C., Szalay, A.S., Szokoly, G.P., Thakar, A.R., Vogeley, M.S., Waddell, P., Weinberg, D.H., York, D.G., The SDSS Collaboration, 2000, AJ, 120, 1198



- Geiger, B. & Schneider, P. 1999, MNRAS, 302, 118
- Griffiths, R.E., Casertano, S., Im, M., & Ratnatunga, K.U. 1996, MNRAS, 282, 1159
- Hoekstra, H. 2000, PhD Thesis, University of Groningen
- Hoekstra, H., Yee, H. K. C. & Gladders, M. D. 2002, astro-ph/0205205
- Hogg, D.W., Cohen, J.G., Blandford, R., Gwyn, S.D.J., Hartwick, F.D.A., Mobasher, B., Mazzei, P., Sawicki, M., Lin, H., Yee, H.K.C., Connolly, A.J., Brunner, R.J., Csabai, I., Dickinson, M., SubbaRao, M.U., Szalay, A.S., Fernandez-Soto, A., Lanzetta, K.M., & Yahil, A. 1998, AJ, 115, 1418
- Hogg, D. W., Pahre, M. A., Adelberger, K. L., Blandford, R., Cohen, J. G., Gautier, T. N., Jarrett, T., Neugebauer, G., & Steidel, C. C. 2000, ApJS, 127, 1
- Hudson, M.J., Gwyn, S. D. J., Dahle, H. & Kaiser, N. 1998, ApJ, 503, 531
- Infante, L. & Pritchett, C. J. 1995, ApJ, 439, 565
- Jaunsen, A. O. 2000, PhD thesis, University of Oslo
- Kochanek, C. S. 2001, astro-ph/0106495
- Keeton, C. R., Kochanek, C. S. & Falco, E. E. 1998, ApJ, 509, 561
- Kormann, R., Schneider, P., & Bartelmann, M. 1994, A & A, 284, 285
- LeFèvre, O., Hudon, D., Lilly, S.J., Crampton, D., Hammer, F. & Tresse, L. 1996, ApJ, 461, 534
- Maller, A. H., Simard, L., Guhathakurta, P., Hjorth, J., Jaunsen, A. O., Flores, R. A., & Primack, J. R. 2000, ApJ, 533, 194
- McKay, T. A., Sheldon, E. S., Racusin, J., Fischer, P., Seljak, U., Stebbins, A., Johnston, D., Frieman, J. A., Bahcall, N., Brinkmann, J., Csabai, I., Fukugita, M., Hennessy, G. S., Ivezić, Z., Lamb, D. Q., Loveday, J., Lupton, R. H., Munn, J. A., Nichol, R. C., Pier, J. R., & York, D. G. 2001, astro-ph/0108013
- McKay, T. A., Sheldon, E. S., Johnston, D., Grebel, E. K., Prada, F., Rix, H.-W., Bahcall, N. A., Brinkmann, J., Csabai, I., Fukugita, M., Lamb, D. Q., & York, D. G. 2002, ApJ, 571, L85
- Natarajan, P., Kneib, J.-P. & Smail, I. 1998, ApJ, 499, 600

- Natarajan, P., Kneib, J.-P. & Smail, I. 2001, in “Gravitational Lensing: Recent Progress and Future Goals”, ASP Conf. Series 237, eds. T. G. Brainerd & C. S. Kochanek, 391
- Natarajan, P. & Refregier, A. 2000, ApJ, 538, L113
- Sackett, P.D. 1999, in “Galaxy Dynamics”, ASP Conf. Series 182, eds. D. R. Merritt, M. Valluri & J. A. Sellwood, 393
- Schneider, P., Ehlers, J. & Falco, E. E. 1992, “Gravitational Lensing”, (Berlin: Springer-Verlag)
- Smail I., Hogg, D.W., Yan, L. & Cohen, J.G. 1995, ApJ, 449, L105
- Smith, D.R., Bernstein, G.M., Fischer, P. & Jarvis, M. 2001, ApJ, 551, 643
- Stewart, G. C., Fabian, A. C., Nulsen, P. E. J., & Canizares, C. R. 1984, ApJ, 278, 536
- Villumsen, J. V., Freudling, W., & da Costa, L. N. 1997, ApJ, 481, 578
- Warren, M. S., Quinn, P. J., Salmon, J. K., & Zurek, W. H. 1992, ApJ, 399, 405
- Wilson, G., Kaiser, N., Luppino, G.A., & Cowie, L.L. 2001, ApJ, 555, 572
- Williams, R. E., Blacker, B., Dickinson, M., Dixon, W. V. D., Ferguson, H. C., Fruchter, A. S., Giavalisco, M., Gilliland, R. L., Heyer, I., Katsanis, R., Levay, Z., Lucas, R., McElroy, D. B., Petro, L., Postman, M., Adorf, H.-M., & Hook, R. 1996, AJ, 112, 1335
- Zaritsky, D. & White, S.D.M. 1994, ApJ, 435, 599
- Zaritsky, D., Smith, R., Frenk, C., & White, S.D.M. 1997, ApJ, 478, 39

**Table 1: Errors Assigned to Post-Lensing Position Angles**

$\epsilon$	$19 < I < 20$	$20 < I < 21$	$21 < I < 22$	$22 < I < 23$
0.0–0.1	30°	30°	30°	35°
0.1–0.2	13°	16°	20°	25°
0.2–0.3	8°	11°	15°	20°
0.3–0.4	4°	6°	8°	10°
0.4–0.5	4°	6°	8°	10°
0.5–0.6	2°	3°	4°	5°
0.6–0.7	2°	3°	4°	5°

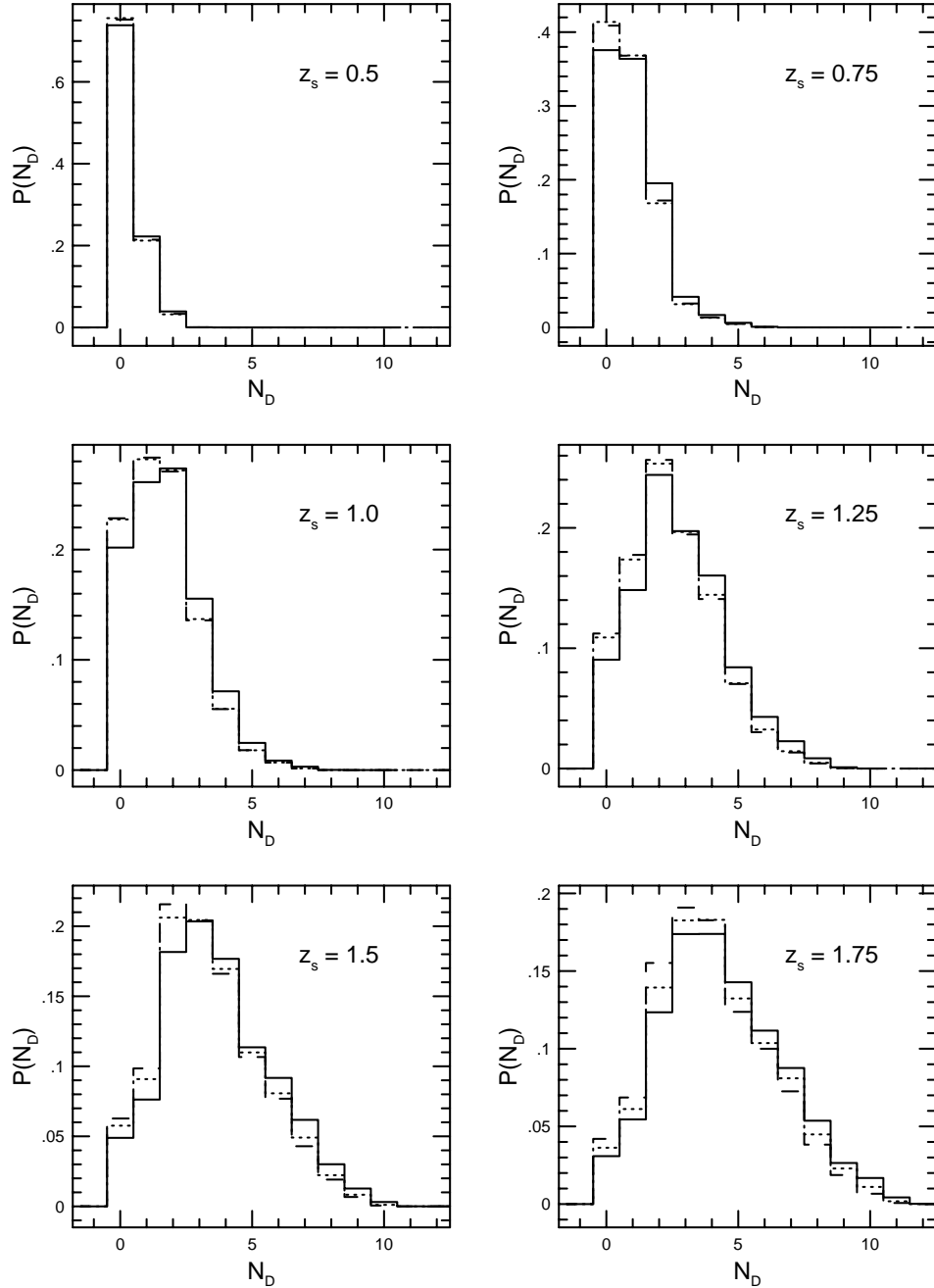


Fig. 1.— Probability distribution of weak lensing deflections for a source galaxy with redshift  $z_s$  that is located in the HDF–N. Only individual deflections which give rise to  $\gamma > 0.005$  are included in  $P(N_D)$ . For sources with  $z_s > 1$ , the probability of multiple deflections (i.e.,  $N_D \geq 2$ ) exceeds 50%. Results are shown for three cosmologies: open (solid line), flat  $\Lambda$ -dominated (dotted line), and Einstein–de Sitter (dashed line).

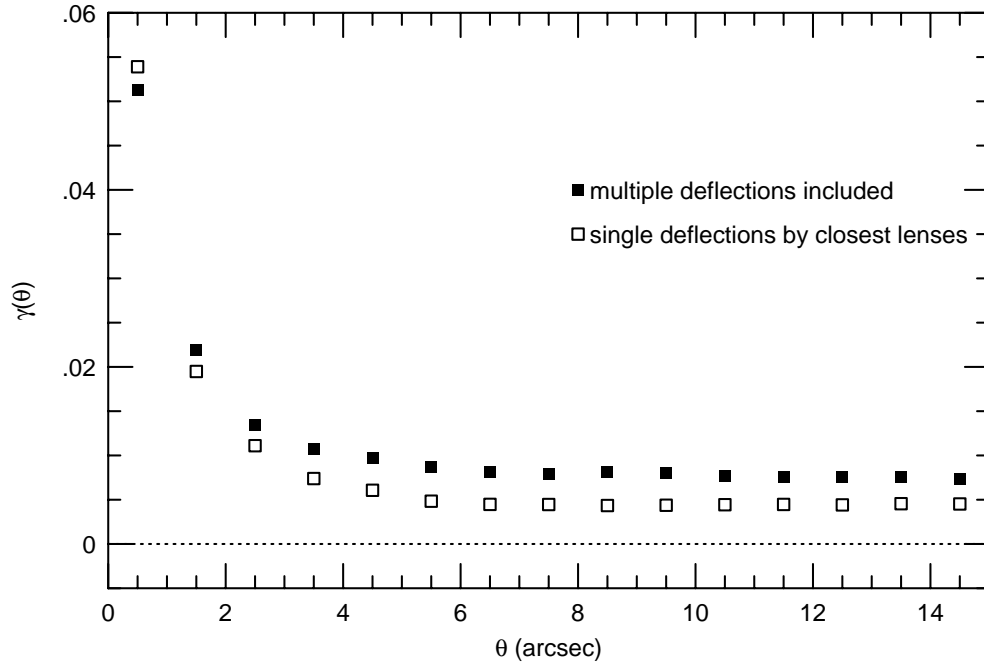


Fig. 2.— Circularly-averaged shear for galaxies in the HDF-N. An open cosmology with  $\Omega_0 = 0.3$ ,  $\Lambda_0 = 0$ , and  $H_0 = 60$  km/s/Mpc has been adopted for this figure, but the results are essentially independent of the choice of cosmology. Solid squares: multiple deflections are used in the determination of the net shear for a given source galaxy. Open squares: only the shear due to the nearest-neighbor lens is used to determine the shear for a given source galaxy. Source galaxies with  $19 < I < 23$  and a magnitude-redshift relation obtained from an extrapolation of the CFRS redshift distribution are used in the calculation (see text).

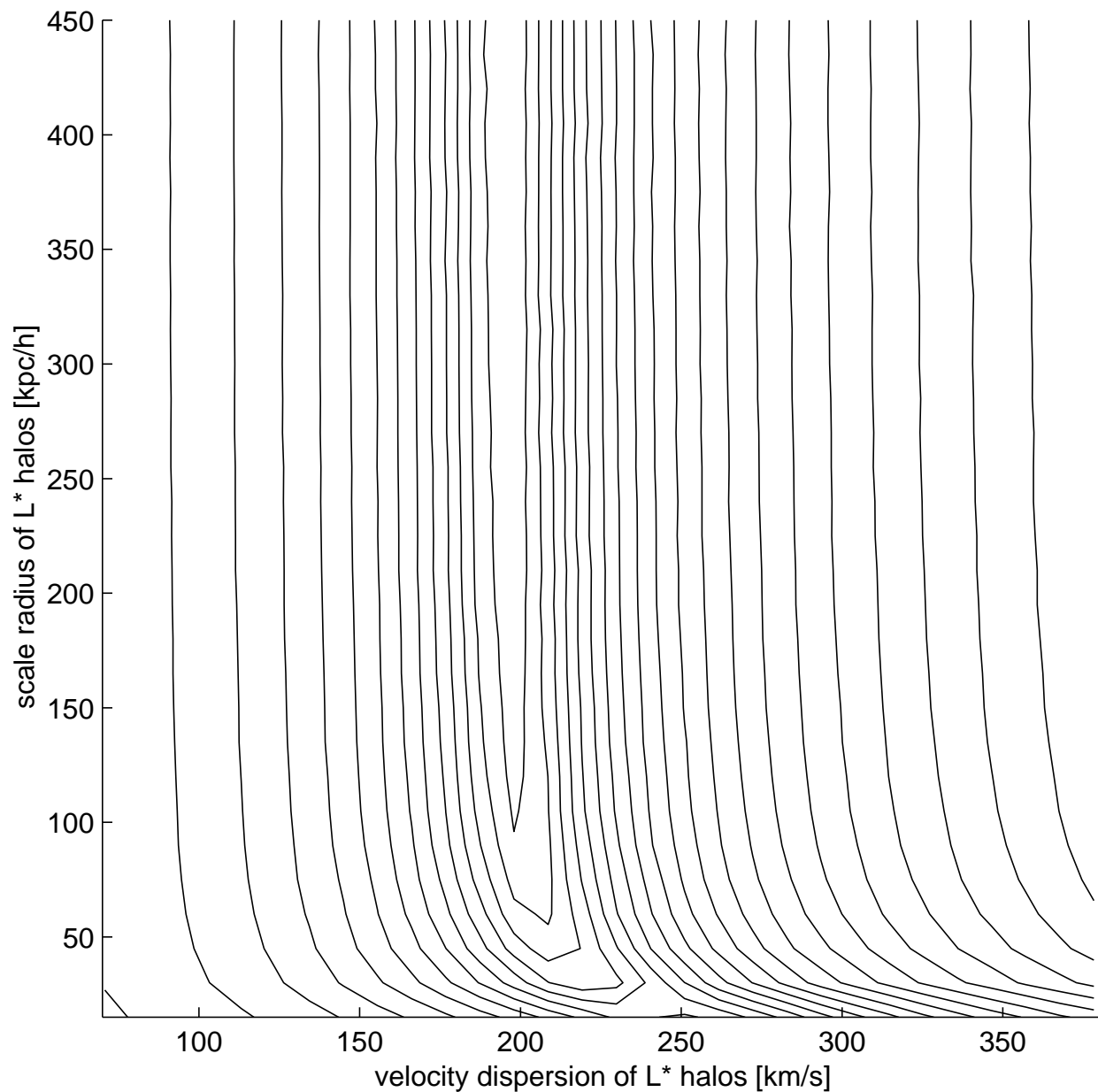


Fig. 3.— Logarithmically-spaced contours of constant  $\chi^2$  for a comparison of  $\gamma(\theta)$  obtained from single-deflection calculations (using various values of  $\sigma_v^*$  and  $s^*$ ) with  $\gamma(\theta)$  obtained from a multiple-deflection calculation in which  $\sigma_v^* = 156$  km/s and  $s^* = 100h^{-1}$  kpc.

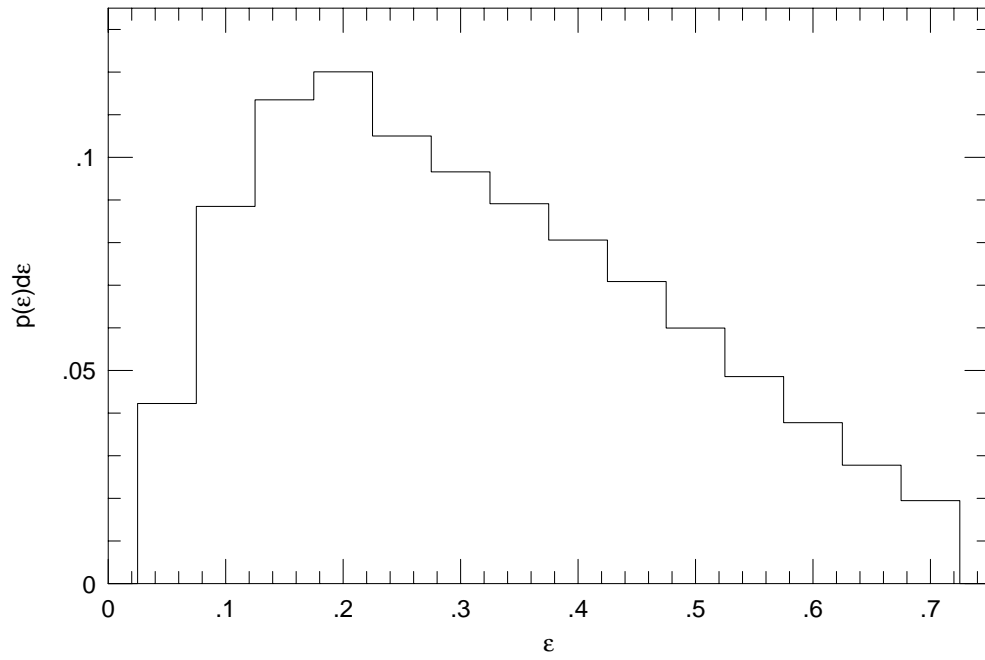


Fig. 4.— The distribution of projected ellipticities of the halos. Here  $\epsilon \equiv 1 - b/a = 1 - f$ .

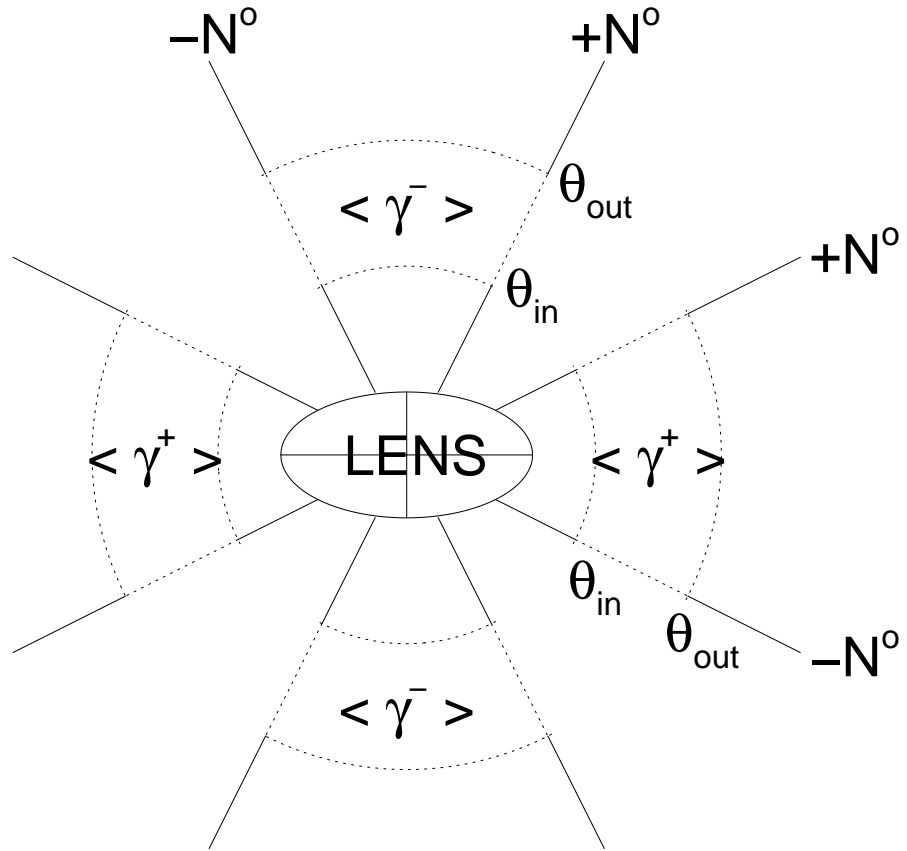


Fig. 5.— Illustration of our notation. The shear experienced by sources located within  $\pm N^\circ$  of the major axis of the lens ( $N \leq 45^\circ$ ) is denoted by  $\gamma^+$  and, similarly, the shear experienced by sources located within  $\pm N^\circ$  of the minor axis ( $N \leq 45^\circ$ ) is denoted by  $\gamma^-$ . Only sources which are located within the dashed regions (defined by the value of  $N$  and by the sizes of the inner and outer angular radii,  $\theta_{\text{in}}$  and  $\theta_{\text{out}}$ ) are used in the calculations of the mean values of the shear,  $\langle \gamma^+ \rangle$  and  $\langle \gamma^- \rangle$ .



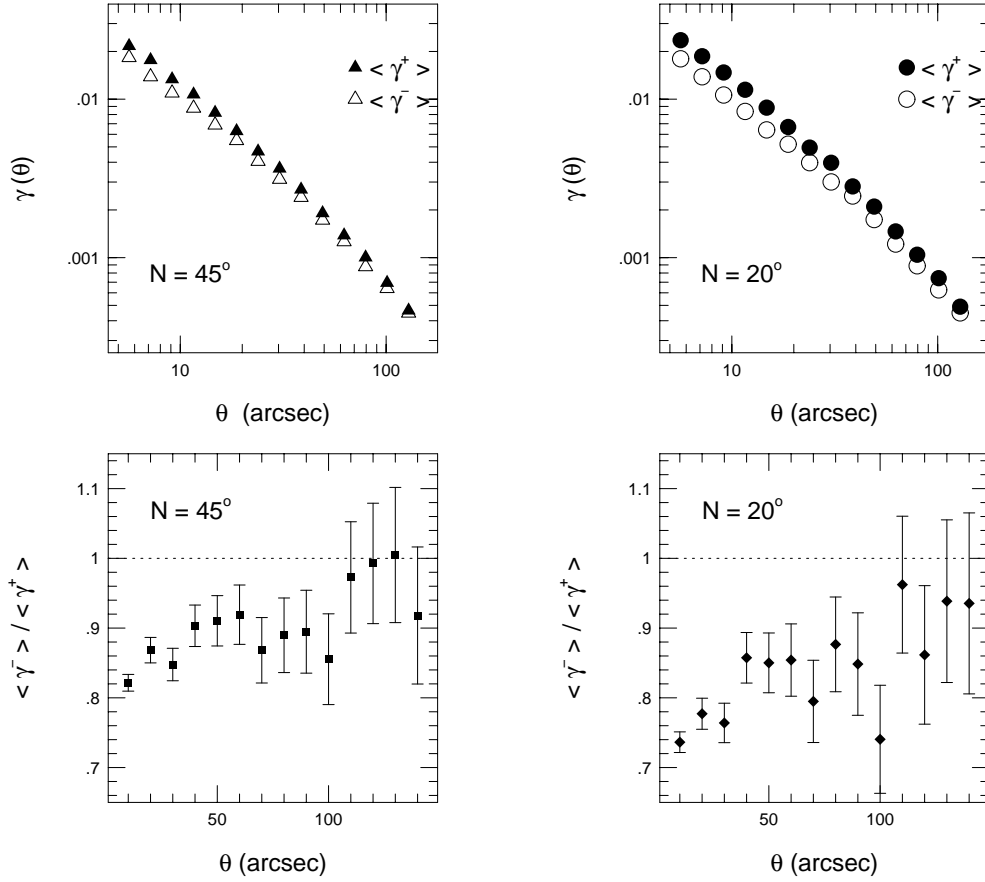


Fig. 6.— The dependence on differential lens–source separation,  $\theta$ , of  $\langle \gamma^+ \rangle$ ,  $\langle \gamma^- \rangle$  (top panels) and  $\langle \gamma^- \rangle / \langle \gamma^+ \rangle$  (bottom panels). Left panels are for the case that all sources have azimuthal coordinates,  $\varphi$ , which are within  $\pm 45^\circ$  of the symmetry axes of the projected halo mass. Right panels are for the case that all sources have azimuthal coordinates,  $\varphi$ , which are within  $\pm 20^\circ$  of the symmetry axes of the projected halo mass. Here, all galaxies with  $19 < I < 23$  are used in the calculation.

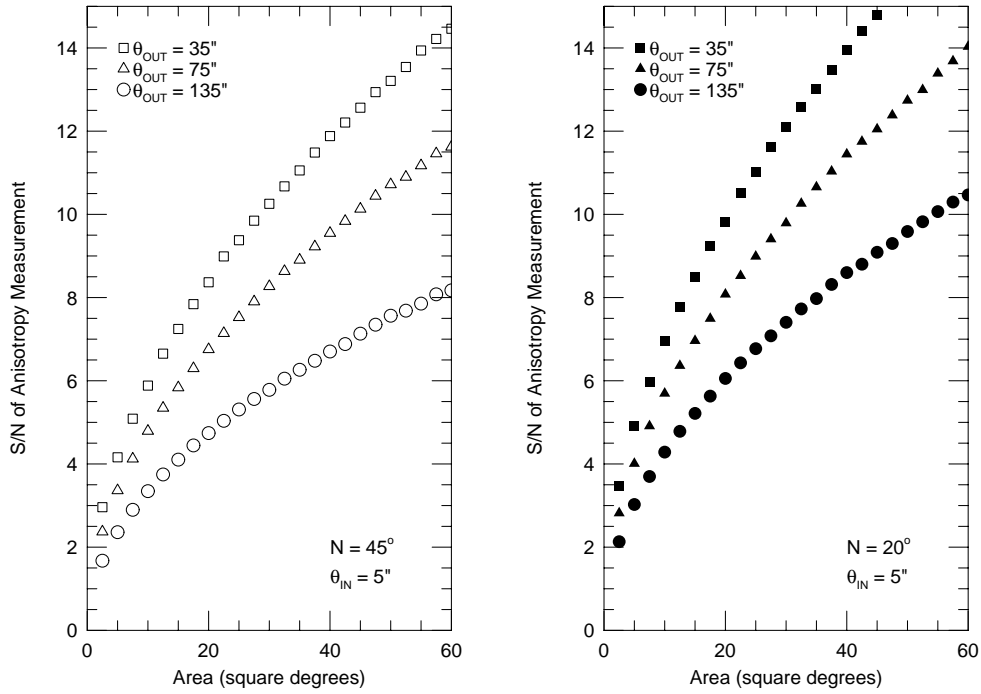


Fig. 7.— The signal-to-noise ratio which can be achieved for a measurement of the anisotropy parameter,  $\mathcal{A}$ , for the case of no observational noise. The left panel shows the results for  $N = 45^\circ$  (measured relative to the intrinsic position angles of the lens galaxies) and the right panel shows the results for  $N = 20^\circ$ . Results are shown for three fiducial analysis annuli:  $5'' \leq \theta \leq \theta_{out}$ ,  $\theta_{out} = 35''$  (squares),  $75''$  (triangles), and  $135''$  (circles).

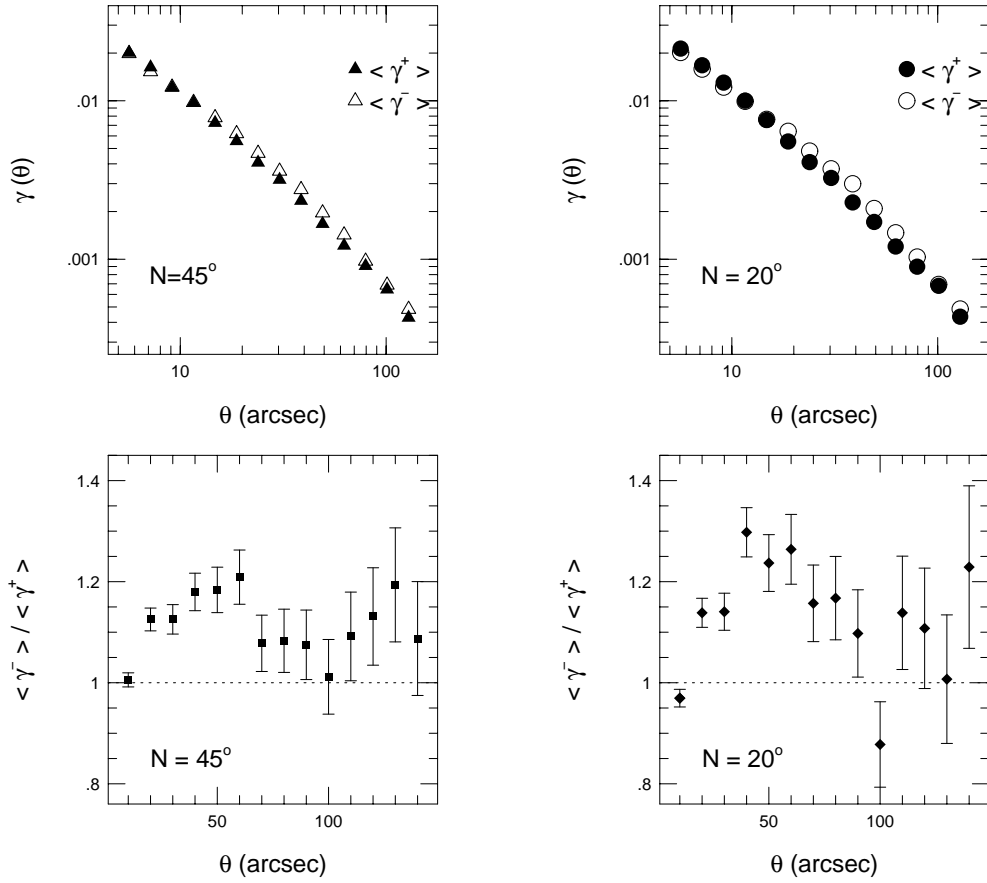


Fig. 8.— Same as for Fig. 6, but here  $N$  is measured relative to the final, post-lensing position angles of the images of the lens galaxies.

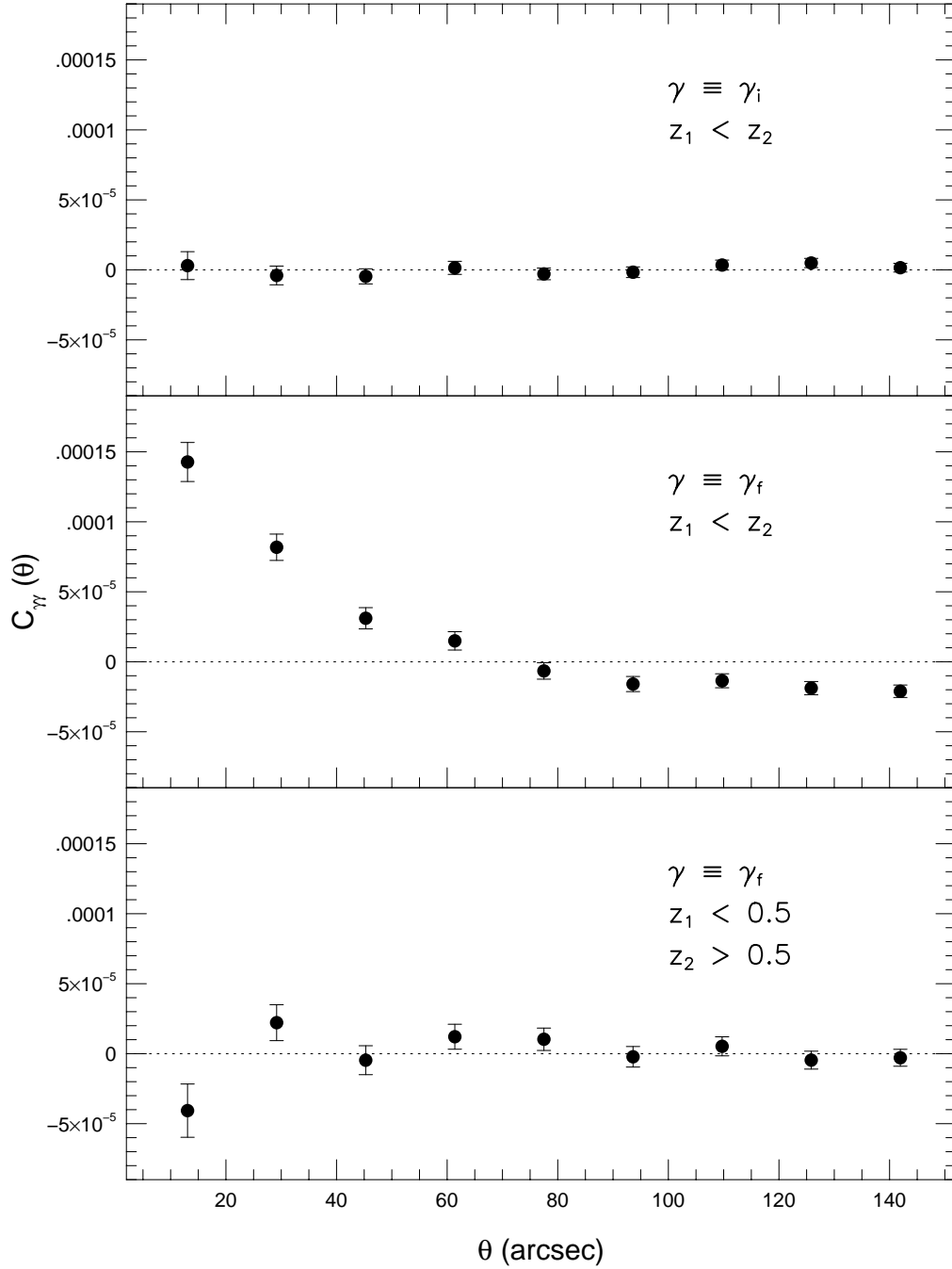


Fig. 9.— The correlation function of image shapes for Monte Carlo galaxies with  $19 < I < 23$ ; i.e., equation (19). Top panel:  $C_{\gamma\gamma}$  computed using the intrinsic shape parameters,  $\vec{\gamma}_i$ , which were drawn at random at the start of each simulation. Middle panel:  $C_{\gamma\gamma}$  computed using the final shape parameters,  $\vec{\gamma}_f$ , after all galaxies had been lensed by all foreground galaxies. Bottom panel:  $C_{\gamma\gamma}$  computed using the final shape parameters for the specific case in which  $z_1 < 0.5$  and  $z_2 > 0.5$ .

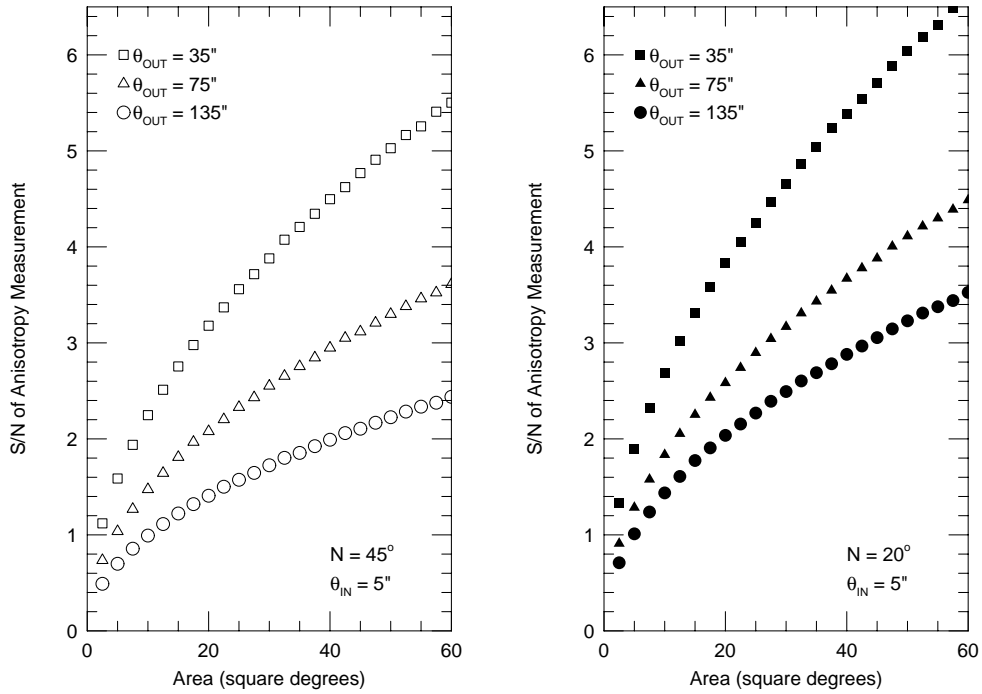


Fig. 10.— Same as Fig. 7, but here  $N$  is measured relative to the final, post-lensing position angles of the images of the foreground galaxies and noise has been added to both the redshifts of the galaxies and the values of the observed position angles (see text and Table 1). Here we restrict the analysis to foreground galaxies with  $z_d^{obs} < 0.5$  and background galaxies with  $z_s^{obs} > 0.5$  in order to break the correlation in the values of  $\vec{\gamma}_f^{obs}$  for foreground–background pairs.

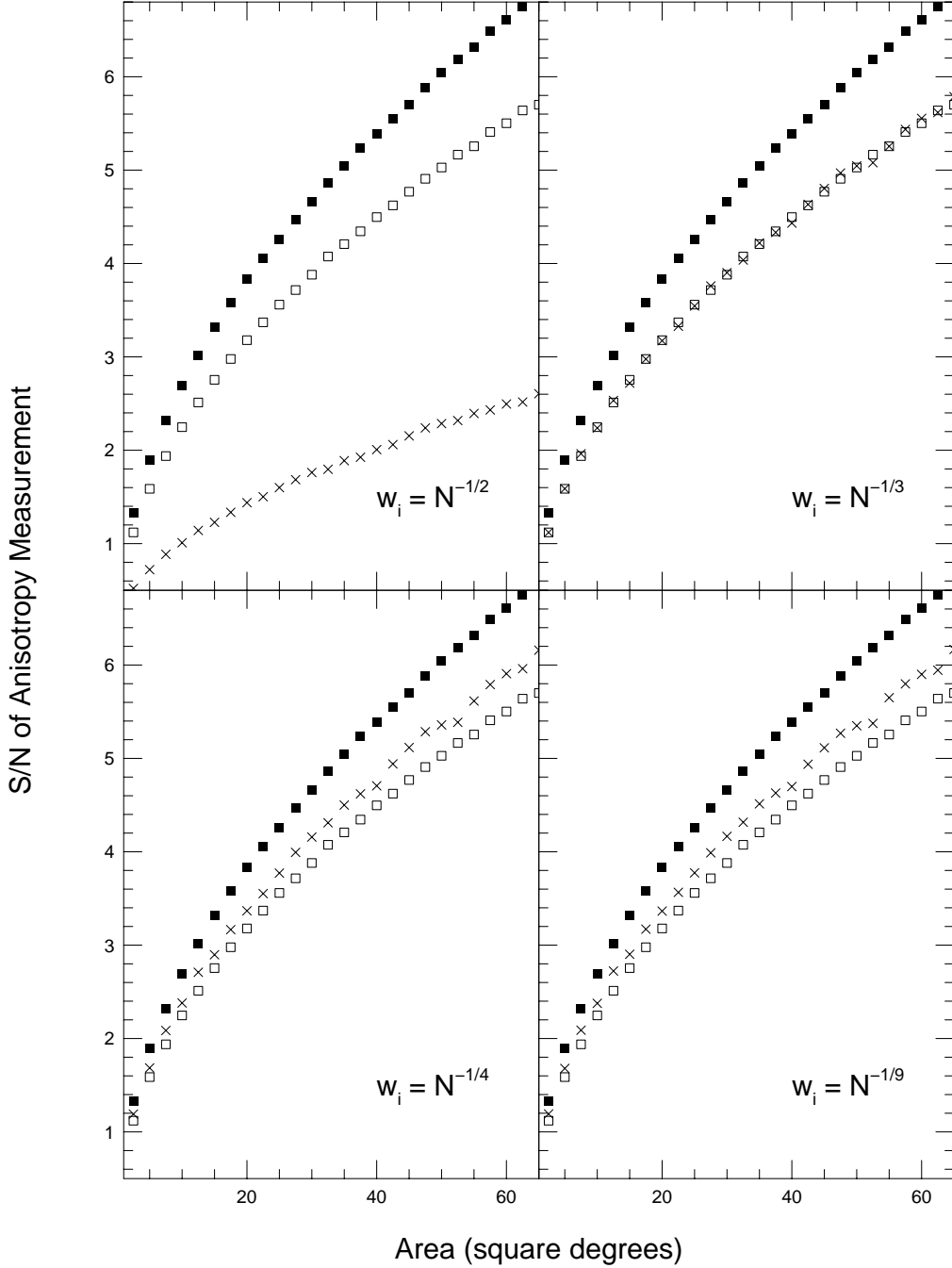


Fig. 11.— Signal-to-noise as a function of survey area for noisy data. Here the signal is averaged over angular scales of  $5'' \leq \theta \leq 35''$  and the azimuthal coordinates of the sources are measured relative to the final, post-lensing position angles of the images of the lenses to which noise has been added. As in Fig. 10 we have restricted the analysis to foreground galaxies with  $z_d^{\text{obs}} < 0.5$  and background galaxies with  $z_s^{\text{obs}} > 0.5$  in order to break the correlation in the values of  $\vec{\gamma}_f$  for foreground-background pairs. Squares show S/N for simple, unweighted means (solid symbols for  $N = 20^\circ$ , open symbols for  $N = 45^\circ$ ). Crosses show S/N for weighted means in which the weights are given by  $N^{-1/2}$  (top left panel),  $N^{-1/3}$  (top right panel),  $N^{-1/4}$  (bottom left panel), and  $N^{-1/9}$  (bottom right panel), where  $N \leq 45^\circ$ .